Assessing carbon storage capacity and saturation across six central US grasslands using data-model integration

Kevin R. Wilcox[1,2], Scott L. ~~Collins[2]~~Collins[3], Alan K. ~~Knapp[3]~~Knapp[4], William ~~Pockman[2]~~Pockman[3], Zheng ~~Shi[4]~~Shi[5], Melinda D. ~~Smith[3]~~Smith[4], Yiqi ~~Luo[5]~~Luo[6,7]

[1]Department of Ecosystem Science and Management, University of Wyoming, Laramie, WY 82071, USA
[2]Department of Biology, University of North Carolina Greensboro, Greensboro, NC, 27412, USA
~~[2]Department~~ [3]Department of Biology, University of New Mexico, Albuquerque, NM, 87131, USA
~~[3]Department~~ [4]Department of Biology & Graduate Degree Program in Ecology, Colorado State University, Fort Collins, CO, 80523, USA
~~[4]Department~~ [5]Department of Microbiology and Plant Biology, University of Oklahoma, Norman, OK, 73019
~~[5]Department~~ [6]Department of Biological Sciences, Center for Ecosystem Science and Society, Northern Arizona University, Flagstaff, AZ, 86011, USA
[7]School of Integrative Plant Science, Cornell University, Ithaca, NY, 14853, USA

Correspondence to: Kevin R. Wilcox (~~kevin.wilcox~~k_wilcox@~~uwyo~~uncg.edu)

Abstract. Future global changes will impact carbon (C) fluxes and pools in most terrestrial ecosystems and the feedback of terrestrial carbon cycling to atmospheric CO_2. Determining the vulnerability of ecosystems to future changes in C is thus vital for targeted land management and policy. The C capacity of an ecosystem ~~(X_C)~~ is a function of its C inputs (*e.g.*, net primary productivity – NPP) and how long C remains in the system before being respired back to the atmosphere ~~(ecosystem C residence time τ_E)~~. The proportion of ~~X_C~~ C capacity currently stored by an ecosystem (*i.e.*, its C saturation ~~C_{SAT}~~) provides information about the potential for long-term C pools to be altered by environmental and land management regimes. We estimated ~~X_C,~~ C capacity, C saturation,~~C_{SAT},~~ NPP, and ecosystem C residence time τ_E in six US grasslands spanning temperature and precipitation gradients by integrating high temporal resolution C pool and flux data with a process-based C model. As expected, NPP across grasslands was strongly correlated with mean annual precipitation (MAP), ~~while yet~~ C residence time τ_E ~~was primarily a function~~not related to MAP or ~~of~~ mean annual temperature (MAT). We link soil temperature, soil moisture, and inherent C turnover rates (potentially due to ~~differences in~~ microbial function and tissue quality) as determinants of τ_E. Overall, we found that intermediates between extremes in moisture and temperature had low ~~C_{SAT}~~C saturation, indicating that ~~ecosystem~~ C in these ~~systems~~ grasslands may trend upwards and ~~may~~ be buffered against global change impacts ~~on X_C~~. Hot and dry grasslands had greatest ~~C_{SAT}~~ C saturation due to both small C inputs through NPP and high C turnover rates during ~~periods of favorable~~ soil moisture conditions favorable for microbial activity. Additionally, leaching of soil C during monsoon events may lead to C loss. ~~C_{SAT}~~C saturation ~~also~~ was also high in tallgrass prairie due to frequent fire that reduced inputs of aboveground plant material. Accordingly, we suggest that both hot, dry ecosystems and those frequently disturbed should be subject to careful land management and policy decisions to prevent losses of C stored in these systems.

1 Introduction

In the coming decades, most terrestrial ecosystems will experience changes in environmental drivers, including increased air temperatures and atmospheric CO_2 concentrations, altered precipitation amounts and patterns, changes in fire frequency, and various anthropogenic impacts (*e.g.*, agriculture)(IPCC, 2022). These changes are likely to have strong impacts on ecosystem functioning, such as C assimilation via plant growth or C losses via respiration (Hungate et al., 1997, Wang et al., 2016, Naylor et al., 2020). These will in turn affect critical ecosystem services, such as C sequestration (Lal, 2004, Wiesmeier et al., 2019). These effects are particularly important in grassland ecosystems due to their global extent (White et al., 2000) and their ability to be sinks for soil C (Conant et al. 2016, Bai and Cotrufo, 2022). Information about grasslands that may experience substantial changes in C storage when subjected to future environmental change is important for targeted land management (Rees et al., 2005) and policy decisions (Daily et al., 2009; Chambers et al., 2016). Experimental studies offer a way to assess how global changes are likely to impact ecosystem processes. Yet, experiments often have difficulty tracking effects on C storage since changes in soil C pools can take decades (Balesdent et al., 1988; Chapin et al., 2011), and most experiments are conducted for relatively short time periods. Process-based models offer another method to assess alterations in soil C under future conditions and have been shown to be useful tools to assess soil C across grasslands (Parton et al., 1993, Bonan et al. 2013). Yet, variation of ecosystem properties and processes controlling C cycling across ecosystems, such as microbial community composition, is not well represented in many current models. Additionally, uncertainty surrounding ecosystem C is currently very large (Todd-Brown et al., 2014, Friend et al., 2014, Luo et al., 2015, Sulman et al., 2018). This highlights the need for better understanding of how C processes vary across ecosystems.

Many estimates of C sequestration rates use two or more time points of C pool measurements to infer annual rates of C accumulation or loss in ecosystems (e.g., Sperow et al. 2016, Smith et al. 2005). While informative, these estimates of C flux rates will not extend indefinitely (Smith 2004), likely due to the non-linear nature of C accumulation or loss through time. (Luo et al. (2017) introduced C capacity (X_C; Table 1) as the amount of C that would be stored in soil and vegetation in an ecosystem if given enough time to reach equilibrium under current environmental conditions. Comparisons of C capacity and the amount of C currently stored by that system allows for predictions of long-term trends of system C and identification of ecosystems that are vulnerable to C loss under global change. In most terrestrial ecosystems, C capacity is primarily a function of C inputs (NPP) and the amount of time that carbon remains in a system before being respired back to the atmosphere (ecosystem C residence time - τ_E, Luo et al., 2017). There are often mismatches between the amount of C currently present within ecosystems and a system's C capacity because recovery from previous disturbances/environmental conditions can take decades or centuries (e.g., tillage, Smith, 2014). This may underlie observations of grasslands acting as strong C sinks (Soussana et al., 2007). The long-term trajectory (e.g., gains or losses) of C in an ecosystem can be inferred through a comparison of its current C storage at present (X_P) with its C capacity (Fig. 1a). It is important to note that the factors influencing C capacity – NPP and C residence time – are constantly changing, and

2

if these changes cause mismatches
between present C and C capacity, this will likely alter long-term C trajectories

70 (Fig. 1b). Alternately, C trajectories where present C is far below capacity may be less vulnerable to
global change scenarios if present C remains below future capacity (Fig. 1c). Therefore, we suggest that
the proportion of C capacity that is currently present in ecosystems (hereafter termed C saturation – C_{SAT}) may be used
as an indicator of how vulnerable C pools are to future changes in environmental drivers.

75 **Table 1. Focal terms, descriptions, and calculation methods used in this study.**

Symbol	Term	Units	Description	Method of calculation
τ_E	Ecosystem C residence time	year	The average amount of time between fixation of a single C molecule and respiration from the soil.	Integrates residence times of six carbon pools, transfer coefficients among pools, soil moisture, soil temperature, and sensitivity of turnover rates to temperature and moisture (Eqn. 1-5). Here, uncertainty of all the above parameters is integrated into estimates of ecosystem C residence time through bootstrapping methods.
NPP	Net primary productivity	g C m^{-2} year^{-1}	The quantity of C produced by plants in one year	Modeled using climate forcing data, benchmarked to empirical observations.
X_C	Carbon capacity	g C m^{-2}	The amount of carbon the ecosystem will contain under continuing steady-state conditions	Multiplication of ecosystem C residence time and net primary productivity. We bootstrapped these estimates to incorporate uncertainty in NPP and ecosystem C residence time.
X_P	Present carbon	g C m^{-2}	How much carbon is currently present in the system	Sum of C in aboveground plant biomass, belowground plant biomass, and the soil. All estimates were based on empirical measurements but extrapolated to 0-20 cm depths in the soil.
C_{SAT}	Carbon saturation	%	The proportion of carbon saturation that is currently present in the system	Carbon capacity divided by the amount of present carbon in the system.
F_T	Temperature scalar	--	Modifies the base C turnover rate dependent on soil temperature	Calculated using soil temperature measurements and the Q_{10} parameter, which is estimated based on empirical data during the data assimilation process.
F_W	Moisture scalar	--	Modifies the base C turnover rate dependent on soil moisture	Calculated using soil moisture measurements and the *mscut* parameter, which is estimated

3

				based on empirical data during the data assimilation process.
ξ	Environmental scalar	--	Modifies base C turnover rates based on soil temperature and soil water content	The effect of water (F_T) multiplied by the effect of temperature (F_W) on C turnover.

Geographic patterns of X_C C capacity depend on how its components (NPP and C residence time)τ_E) vary across vary across ecosystems and environmental gradients. There is robust evidence showing patterns of ANPP along gradients of mean annual precipitation (MAP; Sala et al., 1988, 2012, Burke et al. 1997, 2012, Huxman et al., 2004, Maurer et al. 2020).

80 Yet, root:shoot ratios may be greater in drier ecosystems (Schenk and Jackson, 2002; Zhou et al. 2009, Mokany et al., 2006; Wilcox et al., 2016, Hu et al., 2022), which may result in shallower relationships between MAP and total NPP. Biomass turnover is associated with C residence time a τ_E and has been shown to be an important part of biogeochemical responses to changes in environmental conditions (De Kauwe et al., 2014), yet. tPatterns of turnover of above and belowground plant biomass have been linked with numerous drivers in grasslands, including average temperature (Gill and Jackson 2000),

85 precipitation (Yahdjian et al. 2006), tissue quality (Adair et al. 2008), microbial and fungal decomposer communities (Williams and Rice, 2007; García-Palacios et al., 2016), disturbance (Lorenz and Lal, 2018), and often with interactive effects (Bontti et al. 2009). Yet, our understanding is often clouded by abundant contingencies associated with these patterns, effectively limiting our ability to predict which ecosystems will continue to sequester or release C.

Here, we endeavor to generate process-based understanding about how and why C inputs (e.g., NPP) and losses (C turnover)

90 differ among grassland ecosystems, and then use this understanding to identify grasslands where C losses may occur in the future. within a growing season is often difficult to measure empirically and is missing from many above- and belowground NPP field measurements.

Similar to NPP, there is evidence that respiration rates increase with MAP and MAT due to favorable soil conditions for decomposition (Bird et al., 1996, Carvalhais et al., 2014, Stielstra et al., 2015, Feng et al., 2018), leading to shorter τ_E in

95 warm and wet ecosystems. Additionally, τ_E may be controlled by differences in microbial and fungal decomposer communities (Williams and Rice, 2007; García-Palacios et al., 2016). For example, You et al. (2014) found that the relative abundances of gram-negative bacteria, saprophytic fungi, and actinomycetes had strong impacts on C acquisition and soil organic matter loss in central China forest ecosystems. Currently, information is limited as to how these C input versus output relationships across ecosystems combine to impact X_C along climatic gradients, or how the difference between X_C and

100 X_P (i.e., CSAT) varies.

To do this we (a) assimilated C pool and flux data from six US grassland sites with a process-based ecosystem model (see methods for in depth description of the model) to estimate primary C inputs (NPP), C residence time, and C saturation; and (b) measured present C as the sum of soil and vegetative C to quantify what proportion of C capacity was currently present
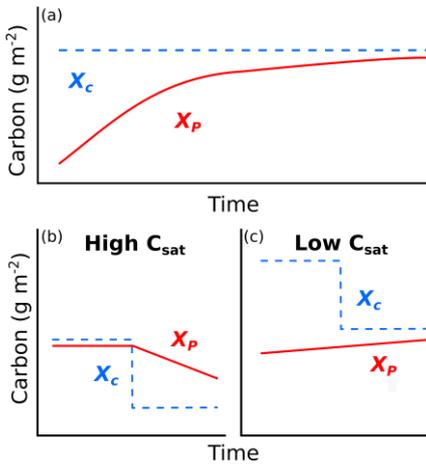
in each of these ecosystems. We address the following questions and predictions:

1. How do NPP, C residence time, and present C vary across gradients of MAP and MAT? We predict that NPP should be primarily related to precipitation since much previous work has shown strong water limitation in grasslands (Sala et al., 1988, Huxman et al., 2004, Maurer et al. 2020), and C residence time will be related to both temperature and precipitation due to strong limitation of these factors on microbial activity.

2. How sensitive is C capacity to turnover rates of different C pools? We predict that changes in turnover rates within slower C pools will have larger effects than faster C pools.

2.3. Is the amount of C present in any of these systems close to their C capacity? We predict that cooler and drier ecosystems will be further from their C capacity. Ecosystems with low moisture and colder temperature have lower productivity and slower turnover of C pools, both of which can slow the rate that present C approaches C capacity.

3. Addressing these questions and hypotheses will provide an initial perspective on how much these key C attributes

Addressing these questions and hypotheses will provide an initial perspective on how much these key C attributes

5

Addressing these questions and hypotheses will provide an initial perspective on how much these key C attributes

120 **Figure 1. (a) Conceptual figure showing how carbon (C) changes through time to approach C storage capacity as a function of the difference between C storage at present (X_P) and C storage capacity (X_C). Changes in C capacity (blue dashed lines in b-c) can be caused by alterations in net primary productivity or ecosystem C residence time. (b) Ecosystems that have present C close to capacity are susceptible to C loss if environmental conditions cause reductions in C capacity, while (c) ecosystems having present C far below capacity may be buffered against C**

125 **losses, at least in the short-term.**

2. Methods

2.1 Site descriptions

We conducted this study at six US grassland sites spanning climatic gradients of mean annual precipitation (MAP) and mean annual temperature (MAT; Table 2). Data collection sites were set up and maintained as part of the Extreme Drought in

130 Grasslands Experiment (EDGE) and represent the major grassland types within the central United States: desert grassland (SBK), shortgrass prairie (SBL, CPER), northern mixed grass prairie (HPG), southern mixed grass prairie (HAR), and tallgrass prairie (KNZ). All sites were ungrazed for at least 10 years before the start of data collection, yet the sites did vary in the length of time between the first year of our measurement and when they were last grazed (SBL and SBK: 39 years, CPER: 15 years, HPG: 10 years, HAR: 9 years,

135 KNZ: at least 30 years). All sites except KNZ were not frequently burned, but KNZ was burned annually to reflect common management in this region (Knapp et al. 1998, Freckleton et al. 2004). See Table 2 and Appendix E for more information about these sites.

Table 2. Site characteristics of each of the six grassland sites in this study.

	Site characteristic	SBL	SBK	CPER	HPG	HAR	KNZ
Climate[a]	Grassland type	Shortgrass prairie	Desert grassland	Shortgrass prairie	Mixed-grass prairie	Mixed-grass prairie	Tallgrass prairie
	Mean annual precipitation (mm)	246	246	375	400	584	892
	Mean growing season precipitation (mm)[b]	163	163	293	303	426	652
	CV of growing season precipitation[b]	48.5	48.5	33.5	32.8	34.7	29.8
	Mean annual temperature (°C)	13.4	13.4	9.5	7.9	12.3	13.0
	Mean growing season temperature (°C)[b]	19.3	19.3	16.4	14.6	20.8	21.4

6

Soil	Bulk density (g cm^{-3})^c	1.68	1.68	1.26	1.18	1.16	1.03
	Field capacity (% soil moisture)^d	27	30	17	29	35	38
	Wilting point (% Soil moisture)^d	7	5	5	10	16	15
Vegetation^e	C$_3$ graminoid (%)	0	0	17.5	53.7	9.0	11.9
	C$_4$ graminoid (%)	48.7	52.0	54.0	27.0	68.9	77.0
	CAM (%)	22.8	0	6.6	0	0.4	0
	Forb (%)	24.2	44.86	19.2	12.5	19.6	8.4
	Woody (%)	3.4	2.3	1.9	5.9	1.2	2.5
	Perennial (%)	82.4	77.5	82.5	95.1	96.6	99.5
	Annual (%)	16.8	21.5	16.6	3.9	2.4	0.4

[a]Climate characteristics are from 1982-2012 weather data, obtained from Knapp et al. 2015
[b]Growing season was defined as April-September for CPER, HPG, HAR, and KNZ, and as April-October for SBL and SBK
[c]Bulk density data obtained from measurements taken at each site in 2015
[d]Estimated using hourly soil moisture data from 2012-2013 in SBL and SBK and from 2013-2015 in CPER, HPG, HAR, and KNZ
[e]Estimated from plant species composition measurements taken during the 2012-2013 growing seasons at SBL and SBK and during the 2014 growing season at CPER, HPG, HAR, and KNZ

140

2.2 Sampling design

For this study, we used measurements of aboveground net primary productivity (ANPP), belowground net primary productivity (BNPP), root standing crop biomass, vegetative litter biomass, soil C, volumetric soil moisture, soil temperature, soil CO_2 efflux, plant species abundance, soil bulk density, and hourly meteorological data. Most of these data were collected from control plots within ~~the EDGE~~ experimental infrastructure, which is a randomized block design having 10 blocks each containing three treatments: one control and two drought treatments; for the purposes of this study, we only use control data from the ten 6 m^2 control plots at each site. See Appendix C for additional details about sampling regimes.

2.3 Estimating GPP and NPP

To generate gross primary productivity (GPP) and net primary productivity (NPP) estimates, we operated the grassland version of the Terrestrial Ecosystem Model (TECO; Weng and Luo, 2008; Shi et al., 2015), which has been shown to produce C flux~~NEE~~ estimates that match observations well in US grassland ecosystems (Shi et al., 2014). TECO is a process-based ecosystem model that has four major sub-models to simulate canopy photosynthesis, plant growth (allocation and phenology), soil water dynamics, and soil carbon turnover based on weather data and site level soil characteristics (Figure A1). To run the model, we used hourly air temperature, relative humidity, vapor pressure deficit, precipitation, and incident photosynthetically active radiation data from nearby weather stations (see Appendix C for additional details about collecting and cleaning meteorological data). GPP and NPP were generated for the main analyses in this paper using TECO for 2012-2014 at SBL and SBK, and for 2013-2015 at the other four sites. Daily GPP estimates were subsequently used to

drive the C sub-model (section 2.4), and annual NPP estimates were used to calculate C capacity (section 2.5). The mismatch in time frame among sites was due to data availability.

160 Formal validation of the vegetation components of the model was conducted at each of the six sites. This was done by calibrating the model for each site based on measured above and belowground plant growth, soil texture, site-level field capacity and wilting point. Then, model spin-up of 500 years (all pools stabilized at each site between 200 and 400 years) was conducted and output from 2014-2017 was compared with observations at each site. Overall, cross-site mean primary production estimates from the model matched empirical observations very well (aboveground biomass R^2=0.99,

165 belowground NPP R^2=0.94). Interannual variability in production from the model was less well correlated with empirical observations, although model predictions most often fell within one standard deviation of empirical observations. (See Appendix D for additional model validation discussion, figures, and tables).

2.4 Optimizing C sub-model parameters

Within the C turnover sub-model in TECO (Fig. A1), parameters for C turnover rates, C transfer rates, and environmental

170 scalars (Table B1) were estimated for each site using data assimilation techniques (Xu et al., 2006; Shi et al., 2015). Compared with benchmarking, this is a more powerful approach for improving model parameterization, but it also requires higher temporal resolution of data to be successful. We used estimated daily GPP, soil moisture, and soil temperature to operate the C sub-model within the data assimilation procedure to optimize the following sets of parameters: (1) six C turnover parameters associated with leaf, fine root, litter, fast SOM, slow SOM, and passive

175 SOM carbon pools, (2) seven C transfer coefficients controlling the proportion of C turnover transferred to other C pools, and (3) two environmental scalars that control C turnover rates based on soil moisture and soil temperature (Table B1). We used a Markov Chain Monte-Carlo method with Metropolis-Hastings algorithm to optimize these parameters . Starting parameter values were obtained from previous studies (Xu et al., 2006, Shi et al., 2015, Zhou et al., 2012) and were . Starting parameter values were obtained from previous studies (Xu et al., 2006, Shi et al., 2015, Zhou et al., 2012) and were

180 . Starting parameter values were obtained from previous studies (Xu et al., 2006, Shi et al., 2015, Zhou et al., 2012) and were allowed to vary uniformly between biologically reasonable bounds (Table B1). Within each iteration, the current set of parameters was tested against a new set of parameters, generated based on the current set of parameters using a step size of 15 with the Metropolis-Hastings Algorithm. Both the current and new set of parameters were used to run the C sub-model with daily GPP estimates (section 2.3), daily measured soil moisture, and daily measured soil

185 temperature from each site. Model output from each of these two runs was then compared with the observations of aboveground vegetation biomass (annually), root standing crop (annually), plant litter (annually), soil C (single measurement), and surface CO_2 efflux (daily). Model performance using the new set of parameters assessed against Metropolis criterion to determine whether the new set of parameters should be kept or discarded. This was done for 360,000 iterations for each of 4 chains within each site to ensure convergence of parameter estimates. Gelman-Rubin (GR) values

8

were mostly < 1.1, with the exception of a few parameters having 1.2 or 1.3 GR values at HPG and HAR (Table B2). All parameters where GR values were high did not converge and drifted slowly over iterations. This resulted in estimates of these parameters close to the midpoint of the parameter bounds, and large uncertainty. To account for this, uncertainty in parameter estimates was incorporated into C residence time estimates via bootstrapping methods (see below). Cross-correlations were calculated for all parameters at each site (Table B3). Maximum likelihood estimates (MLE) and uncertainty (95% confidence intervals) were calculated for each parameter at each site by assessing normal, log-normal, or Weibull distributions depending on the magnitude and direction of skew (Fig. A2-A4, Table B2).

2.5 Estimating C residence time, C capacity and C saturation

We calculated ecosystem C residence time (τ_E) following Luo et al. (2017):

$$\tau_E = (A\xi(t)K)^{-1}B \tag{1}$$

, where ξ(t) represents the environmental scalar determined by soil moisture and soil temperature at time step t, A is a matrix of C transfer coefficients, K is a 6x6 diagonal matrix representing rates of C loss per day from each of the six C pools, and B is a 6x1 matrix representing the allocation fractions of GPP to each of the six C pools:

$$\xi(t) = F_T(t)F_W(t); \tag{2}$$

$$A = \begin{pmatrix} -1 & 0 & 0 & 0 & 0 & 0 \\ 0 & -1 & 0 & 0 & 0 & 0 \\ 1 & 1 & -1 & 0 & 0 & 0 \\ 0 & 0 & f_{4\leftarrow3} & -1 & f_{4\leftarrow5} & f_{4\leftarrow6} \\ 0 & 0 & f_{5\leftarrow3} & f_{5\leftarrow4} & -1 & 0 \\ 0 & 0 & 0 & f_{6\leftarrow4} & f_{6\leftarrow5} & -1 \end{pmatrix}; \tag{3}$$

$$K = \begin{pmatrix} c_1 & 0 & 0 & 0 & 0 & 0 \\ 0 & c_2 & 0 & 0 & 0 & 0 \\ 0 & 0 & c_3 & 0 & 0 & 0 \\ 0 & 0 & 0 & c_4 & 0 & 0 \\ 0 & 0 & 0 & 0 & c_5 & 0 \\ 0 & 0 & 0 & 0 & 0 & c_6 \end{pmatrix} \tag{4}$$

$$B = (X_A, X_B, 0, 0, 0, 0) \tag{5}$$

In Eqn. 2, F_T is the effect of soil temperature on microbial decomposition rates at time t: $Ft(t) = 0.58Q_{10}^{(T(T)-10)/10}$, where Q_{10} is a constant parameter and T is soil temperature. F_W is the potential effect of soil water content on microbial decomposition rates at time t: $Fw(t) = 1 - 5(mscut-W(t))$, where *mscut* is a constant parameter representing the soil water content (W) below which microbial decomposition becomes limited. If W is greater than *mscut*, $F_W = 1$. The impact of F_T and Fw scalars on ξ

9

are dependent on one another (*i.e.*, F_W will limit ξ in dry conditions even if soil temperatures lead to a large F_T). In Eqn. 3, $f_{i \leftarrow j}$ represents the fractions of C turnover entering pool i pool from pool j. In Eqn. 4, c_{1-6} represents the amount of carbon lost from pools 1-6 per day, where pool 1=aboveground plant biomass, 2=belowground plant biomass, 3=fine litter biomass, 4=active (fast) soil organic matter (SOM), 5=slow SOM, 6=passive SOM. In Eqn. 5, X_A and X_B are the fractions of GPP allocated to aboveground and belowground vegetative pools, respectively. For each site, X_A and X_B were estimated from observed ANPP:BNPP ratios, and data assimilation was used to estimate c_{1-6}, $f_{i \leftarrow j}$, Q_{10}, and *mscut* parameters. To generate uncertainty surrounding τ_E, we bootstrapped 1000 parameter sets from the Markov chain Monte Carlo (MCMC) and obtained the MLE and 95% confidence intervals from the resulting distribution of τ_E estimates.

C capacity (X_C) was calculated following Luo et al. (2017) as:

$$X_C = NPP \cdot \tau_E \qquad (6)$$

, where NPP is net primary productivity of a site, obtained via TECO simulations, and τ_E is the MLE of the distribution of bootstrapped τ_E values. C capacity estimates were obtained by combining the boostrapped iteration of C residence estimates with 1000 randomly sampled values of NPP using the mean and standard deviation of NPP across years. This allowed us to propagate the uncertainty present in both NPP and C residence time to C capacity estimates. The 1000 boostrapped iterations were then used below in the calculation of C saturation.

At KNZ, NPP in Eqn. 6 consisted only of the belowground component because annual fire removes all aboveground plant material each spring. We recognize the limitation of using three years of NPP data to estimate X_C, yet we believe it is important that NPP and τ_E estimates are derived from the same time periods, and the data necessary to estimate τ_E were only available for three years. Weather within the three focal years was comparable to long-term averages at most of the sites (Fig. A5), although precipitation was greater than the long-term average at HPG, lower than the long-term average at HAR, and air temperatures were warmer at SBK and SBL in 2012-2014. Standard deviation of C residence time (C_{sd}) was calculated as the standard deviation of the 1000 bootstrap iterations.

The level of C saturation (C_{SAT}) represents the percentage of C capacity that is represented by present C, calculated as

The level of C saturation (C_{SAT}) represents the percentage of C capacity that is represented by present C
, calculated as

$$C_{SAT} = \frac{c_S + c_A + c_B}{x_C} \qquad (7)$$

, where C_S is the mass of C in the soil standardized by area, C_A is the observed aboveground biomass * 0.45, and C_B is the observed root biomass * 0.45, also standardized by area. Combined, C_S, C_A, and C_B make up present C from 0-10 cm

10

in the soil. Soil C measurements from 0-10 cm in the soil were then extrapolated to 0-20 cm to match up with the depth of BNPP observed and used to calibrate the model. This was done by extracting soil C data along a depth profile (0 to >1 m depth) from the international soil carbon network (ISCN; Nave et al 2017) in nearby areas having similar cover types and land management regimes (Table B4). These depth profiles were used to calculate the proportion of soil C across depths using a beta distribution described by Jobággy and Jackson (2000)(Fig. A7). Then, each soil C measurements from 0-10 cm was extrapolated along this curve to estimate the amount of soil C from 0-20 cm (Fig. A7). The mean and standard deviation among replicates within a site were used to generate 1000 random draws from a normal distribution. We then combined these random draws with the bootstrap iterations from Eqn. 6 to propagate the uncertainty of C capacity (X_C) into the estimate of C saturation. This means that all levels of uncertainty, from individual parameter estimates (Fig. A2-A4) all the way through present C are incorporated into our estimates of C saturation.

We conducted variance partitioning to determine the amount of cross-site variance in C capacity that was driven by variation in NPP versus C residence time. Since only BNPP was incorporated into the X_C calculation for KNZ, we performed this analysis both with and without KNZ (Fig. A6).

2.6 Sensitivity analyses

For each parameter used to calculate C residence time, we varied the parameter while keeping all other parameters constant at their MLE and recorded the resulting C residence time. We did this for 20 intervals ranging from the minimum to maximum parameter values shown in Table B1. We also wished to determine the impact of each parameter value at each site as estimated via data assimilation. To this end, we shifted each parameter from its default value (Table B1) to the MLE value obtained from data assimilation (Table B2) – holding all other parameters at their default values – and observed the resulting effect on C residence time (Fig. 3g-l).

2.7 Statistical analyses

For regression analysis comparing NPP, C residence time, and present C across gradients of MAP, and MAT, all variables were centered by their mean and scaled by their standard deviation, allowing for comparable slope values.

Additional site-level characteristics (Bulk density, grass:forb, C_3:C_4, Annual species abundance) were combined with climate data using partial regression and adjusted R^2 values were assessed to test whether climate-NPP or climate-C residence time relationships were being driven by other site-characteristics (vegan package, Oksanen et al. 2016). Bayesian data assimilation and bootstrapping analyses were run using custom scripts; linear regression models were run with the lm() function. All analyses were conducted in R (R core team, 2022).

11

3 Results

3.1 Net primary productivity (NPP) and present C (X_P)

Estimates of NPP varied across sites from 45.3 g C m^{-2} yr^{-1} at SBL to 400.2 g C m^{-2} yr^{-1} at KNZ (Table 3). The standardized full NPP model (NPP ~ MAP + MAT) was significant ($F_{2,3}$=63.8, P<0.01) and explained 96% of the cross-site variation in NPP estimates (Adj. R^2 = 0.96). Within the model, MAP was strongly correlated with NPP across sites ($F_{1,3}$=123.7, P<0.01), while the relationship with MAT was not significant ($F_{1,3}$=0.58, P=0.50)(Fig. 2). The non-standardized relationship between MAP and NPP was of the form $NPP = 0.53*MAP - 51.4$. We looked for collinearity of MAP with soil bulk density, grass:forb, C_3:C_4, and annual species abundance using partial regression analysis. We found that MAP was still a significant and strong predictor of NPP when these other variables were accounted for (Table B5). Similarly, we found a weak positive relationship between present C and MAP ($F_{1,3}$=6.59, P=0.08, Adj. R^2=0.54), and no relationship between MAT and present C (Fig. 2). The non-standardized relationship between MAP and present C was of the form $X_P = 767.4 + 4.0*MAP$.

Table 3. Estimates (μ and q_{50}) and uncertainty (σ and other quantiles) of NPP and ecosystem carbon residence time at all six sites.

Site		C residence time (τ_E)(years)						NPP (g C m^{-2})	
	$q_{2.5}$	q_5	q_{25}	q_{50}	q_{75}	q_{95}	$q_{97.5}$	μ	σ
SBL	5.2	7.1	18.3	35.3	68	175.1	238.1	45.3	15.3
SBK	11.4	13.2	20.4	27.8	37.7	58.5	67.5	67.7	27.5
CPER	19.1	22.5	36.8	51.8	72.9	119.2	139.9	143.5	25.0
HPG	21.2	25.2	42.5	61.3	88.2	149.2	176.9	157.5	65.1
HAR	17.3	21.1	39.9	59.9	91.9	170.2	207.9	173.2	31.8

12

| KNZ | 9.9 27.76 | 11.9 | 20.71 0.23 75.31 | 30.41 2.01 64.14 | 44.7 | 77.81 9.69 39.13 | 93.2 | 400.2 0682 | 140.9 7561.0 |

285

3.2 Ecosystem carbon residence time (τ_E)

Estimates of ~~τ_E~~ C residence time were obtained by calculating the 50th percentile of the lognormal distribution of bootstrapped C residence time values. These estimates ranged across sites from ~~26.6~~27.8 years ~~in~~ at SBK to ~~54~~61.3~~2~~ years ~~in at CPER~~ HAR (Table ~~2~~3). The standardized full ~~τ_E~~ C residence time model ($\tau_E \sim$ MAP + MAT) ~~was less robust than that of NPP~~was not significant ($F_{2,3}$=~~3.3~~2.05, P=~~0.18~~0.27). Within the full model, neither MAP ($F_{1,3}$=0.10, P=0.77) nor MAT ($F_{1,3}$=4.10, P=0.14) ~~was~~ were ~~not~~ correlated with C residence time ~~τ_E~~ across sites ~~($F_{1,3}$=0.13, P=0.74), while the relationship with MAT was only significant at α=0.1 ($F_{1,3}$=6.57, P=0.08)~~(Fig. 2b). ~~The non-standardized relationship between MAT and τ_E was of the form $\tau_E = -3.6*MAT + 81.6$. Based on partial regression, underlying relationships with other site-based variables were not driving the relationship between MAT and τ_E (Table B5).~~

295
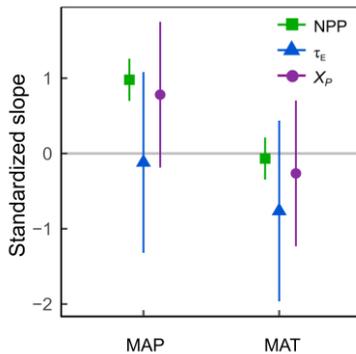
Figure 2. Slopes between standardized net primary productivity (NPP), ecosystem C residence time (τ_E), or present C (X_P) and standardized mean annual precipitation (MAP) and mean annual temperature (MAT). Error bars represent ~~90~~95% confidence intervals.

300

3.3 Soil moisture and temperature effects on C residence time ~~τ_E~~

All sites exhibited a cyclical pattern of soil moisture and temperature effects on C turnover rates (denoted ξ), with higher ξ during the growing season due to warmer temperatures (Fig. 3 black lines). ξ during the growing season was > 1 for all sites

13

except CPER, meaning that C turnover rates were increased in the data driven model, rather than limited by soil conditions. At SBL and SBK (Fig. 3a,b), temperature constraints (F_T; Fig. 3 dashed orange lines) on ξ were > 1 for much of the growing

305 season, yet ξ was limited by soil moisture constraints (F_W; Fig. 3 dotted blue lines) outside of the monsoon season. Only when monsoon rains removed soil moisture limitations did ξ generally persist above one. At CPER (Fig. 3c), ξ was not limited by F_W. Yet, F_T was < 1 throughout the year due to the low Q_{10} value estimated for CPER (Table B2). F_T was much greater than one during the growing season at both the mixed grass and tallgrass prairie sites (Fig. d-f), but F_W limited ξ at both mixed grass prairies. ξ was high at KNZ due to a lack of F_W effect at the site, which was a result of both high soil

310 moisture content throughout the growing season, and a relatively low estimated *mscut* parameter value (Table B2).

14
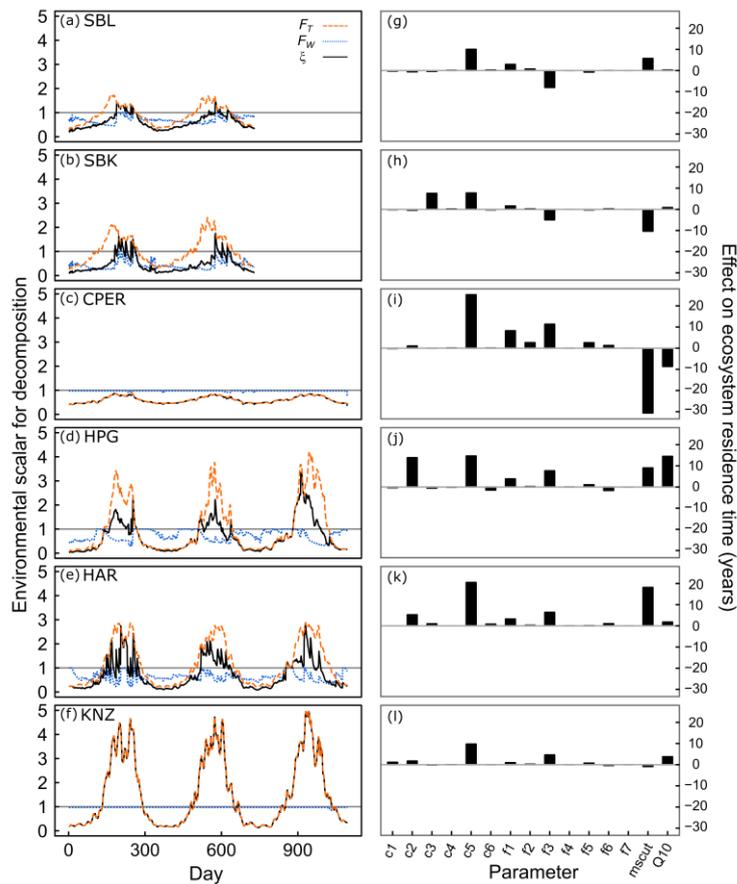
Figure 3. Environmental scalars for decomposition rates at six grassland sites (a-f) and impact of individual parameter estimates on ecosystem carbon residence time (g-l). In a-f, values less than 1 represent soil conditions limiting decomposition while values greater than 1 represent acceleration of decomposition due to soil conditions. Dashed orange lines represent the temperature scaling effect (F_T) – based on the site-estimated value of the Q_{10} parameter and daily soil temperature data. Dotted blue lines represent the moisture scaling effect (F_W), which is based on the site-estimated value of the *mscut* parameter and daily soil moisture data. Black solid lines represent the product of the temperature and moisture scalars (ξ), which is the overall environmental scalar that controls decomposition rates in the model. In g-l, parameters were shifted one at a time from their mean parameter space (baseline parameter) to the parameter estimates obtained from data assimilation, and the resulting effect on ecosystem carbon residence time is

shown. This represents the inherent effect of each model parameter on τ_E independent from soil moisture or temperature. Panels correspond to different sites: a,g=Sevilleta National Wildlife Refuge blue grama grassland; b,h=Sevilleta National Wildlife Refuge black grama grassland; c,i=Central Plains Experimental Range; d,j=High Plains Grasslands Research Station; e,k=Hays Agricultural Research Center; f,l=Konza Prairie Biological Station. Transfer parameters ($f_{x \leftarrow y}$) dictate the proportion of C turnover in pool y transferring to pool x: f1=f4←3; f2=f5←3; f3=f5←4; f4=f6←4; f5=f4←5; f6=f6←5; f7=f4←6.

3.4 Sensitivity of C residence time to model parameters

We performed two sensitivity analyses to (1) identify variables in the model with potential to contribute the most to τ_E (Fig. 4), and (2) quantify the realized effect of model parameter estimates, obtained through the data assimilation process, on C residence time at each site (Fig. 3). These sensitivity analyses simulated C residence time under a range of parameter values while incorporating daily soil temperature and moisture measurements from each site. We found that C turnover rates of the slow and passive SOM pools had the potential to have the greatest impacts on C residence time, highlighting the importance of C sequestration in these pools for maintaining C stocks (Figure 4). C residence time was also sensitive to the *mscut* parameter, with the effect increasing exponentially until reaching ca. field capacity at each site. In the drier sites (SBL, SBK, and CPER), the effect of the *mscut* parameter started to increase rapidly around 10-15% volumetric soil moisture. The steep increase began at greater soil moisture levels (20-25%) at the more mesic sites (HPG, HAR, KNZ). At the warmer sites (SBL, SBK, KNZ), C residence time was less sensitive to Q_{10}, unless Q_{10} was very low (ca. 1). Interestingly, higher Q_{10} values had the potential to increase C residence time at the cooler sites (CPER, HPG). Although Q_{10} is generally negatively related to C residence time, the form of the Q_{10} relationship is such that, although lower Q_{10} values result in slower turnover rates at high soil temperatures, they also result in higher turnover rates under cooler temperatures due to their shallower slope. As such, this can lead to a positive relationship between Q_{10} values and C residence time at cooler sites.

When we applied the estimated parameters to these sensitivity curves to estimate the actual effect of individual parameters on the C residence time estimates (Fig. 3 right panels), we found that turnover rates of the slow SOM pool increased C residence time greatly compared with starting parameters across all sites (+8 to +25 years). Root turnover had a substantial effect on C residence time at HPG (+14 years) and HAR (+5 years). The transfer proportion from fast SOM to slow SOM had a positive effect on C residence time at CPER, HPG, HAR, and KNZ (+5 to +11 years), and a negative effect on C residence time at SBL and SBK (-5 to -8 years). *mscut* had opposite effects on C residence time for SBL (+6 years) than SBK (-10 years), while Q_{10} had minimal effects at both sites. *mscut* and Q_{10} had strong negative effects on C residence time at CPER (-31 years and -9 years, respectively), likely due to particularly low *mscut* and Q_{10} estimated for that site (Fig. A4) and strong potential for impact of these parameters at CPER (Fig. 3). At the other cool site, HPG, both

16

mscut and Q_{10} increased C residence time (+9 and +14 years, respectively). At HAR, a high *mscut* estimate increased C residence time (+18 years), suggesting that C turnover at this site may be particularly sensitive to soil moisture. Q_{10} estimated at HAR had minimal impact. *mscut* and Q_{10} estimates at KNZ had small impacts on C residence time (-1 and +4 years, respectively, Fig. 3).
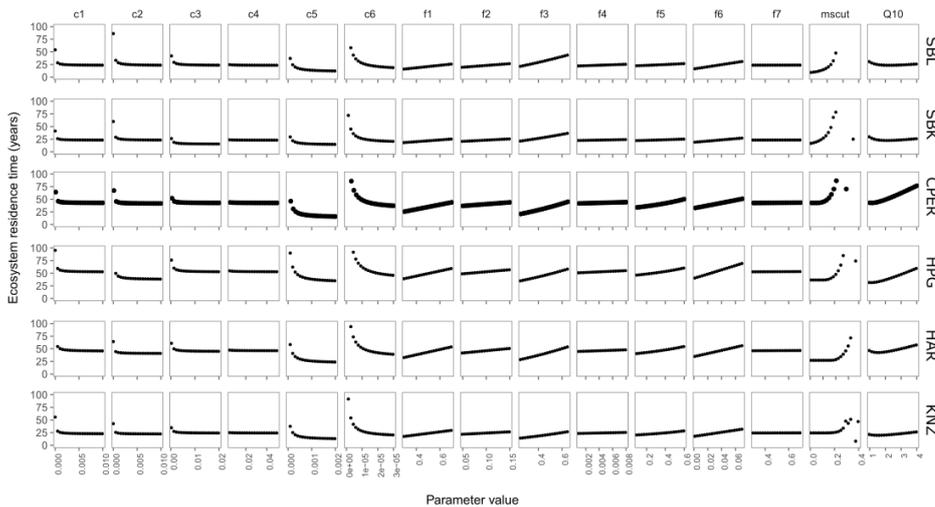
Figure 4. Results from sensitivity analysis where ecosystem C residence time was calculated when altering one parameter value at a time. Rows of panels correspond to different sites with: SBL= Blue grama dominated site at the Sevilleta National Wildlife Refuge; SBK= Black grama dominated site at the Sevilleta National Wildlife Refuge; CPER=central plains experimental range; HPG=High Plains Grassland Research Station; HAR=Hays Agricultural Research Station; KNZ=Konza Prairie Biological Station. Ecosystem carbon residence time was often very high at very extreme parameter values so the y axis was set for clarity. Transfer parameters (f1-7) are as in Fig. 3.

3.5 Carbon capacity and carbon saturation

Finally, we used NPP and C residence time estimates to calculate C capacity. Cross-site variation of NPP and C residence time were both important for determining C capacity across the six grassland sites (Fig. A6). Median C capacity varied from as little as 1,485 g m^{-2} in SBL to as much as 10203 g m^{-2} in HAR (Fig. 5). We estimated C saturation as the percentage of C capacity made up by present C. In the two hot and dry sites (SBL and SBK), we found that C capacity was relatively small and less than present C (Fig. 5), resulting in greater C saturation values (50th percentiles of C saturation lognormal distribution: SBL 148%, SBK 130%, Fig. 5 inset). The cooler and/or wetter sites all had greater C capacity

17

values and present C below capacity (Fig. 5), resulting in smaller C saturation values (50th percentiles: CPER 36%, HPG 56%, HAR: 58%, Fig. 5 inset). The exception to this was KNZ, the most mesic but frequently burned site with a C saturation value of 137% (50th percentile, Fig. 5 inset).
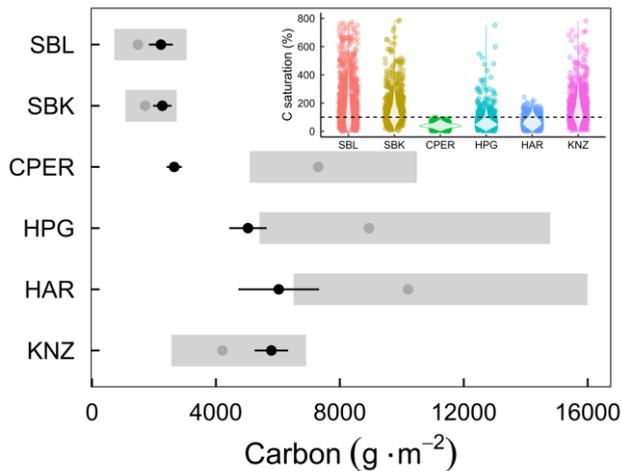
Figure 5. Ecosystem C capacity (X_C; grey points) and present C (X_P; black points) in six grassland ecosystems. Present C was calculated using estimates of soil C from 0-20 cm + aboveground and belowground vegetative C. Black error bars represent one standard deviation around the mean, and grey rectangles represent the 25th and 75th percentiles of the lognormal distribution of C capacity, surrounding the 50th percentile (grey points). Inset: Violin plots and bootstrap estimates of C saturation, calculated as present C divided by the product of NPP and ecosystem C residence time. The dashed line shows where present C is equal to C potential.

4. Discussion

Our findings provide insights for the three questions we posed at the start of this study: (1) How do NPP, C residence time, and present C vary across gradients of MAP and MAT? (2) Is present C in any of these systems close to C capacity? and (3) How does the level of C saturation vary across these grasslands? Related to our first question, we found general support for the prediction that NPP and present C exhibited positive relationships with MAP, yet found no relationship between ecosystem C

18

residence time and climate or other site-level characteristics. Instead, the cross-site pattern of C residence time was driven by differences in local edaphic environments (soil moisture and soil temperature) as well as inherent differences in turnover rates, which may be indicative of biological or physical differences across sites (Baisden et al., 2013, Mathieu et al., 2015, Doetterl et al., 2015, Zhao et al., 2021). Related to our second and third questions, we found that three of these grasslands had particularly high C saturation values, indicating vulnerability to C change in the future and a limited ability of these systems to be long-term C sinks. Two of these three grasslands were in hot, dry climates where C turnover rates were high and C inputs through NPP low. The third grassland (KNZ) was the most mesic and had the highest levels of productivity, yet annual burning at KNZ increased C saturation substantially. Below, we discuss these findings in more detail.

4.1 Relationships of NPP, C residence time, and present C with climate

Abundant research exists showing spatial relationships between ANPP and climate. Sala et al. (1988) was able to explain 90% of the cross-site variation in averaged ANPP with mean annual precipitation across the Great Plains. Yet, total NPP (ANPP + BNPP) is a better determinant of C processes due to large contributions of root C to soil pools (Sulzman et al., 2005; Guzman and Al-Kaisi, 2010; Leppälammi-Kujansuu et al., 2014). A potential reason why BNPP and total NPP relationships with climate may be less clear than ANPP relationships is that, in wetter ecosystems, plants tend to allocate less carbohydrates to roots and more to aboveground material (Schenk and Jackson, 2002, Mokany et al., 2006, Zhou et al. 2009, Wilcox et al., 2016, Hu et al., 2022). This pattern results in a weaker relationship between MAP and NPP than predicted by ANPP-MAP relationships since BNPP is proportionally greater in drier ecosystems. Indeed, we found some evidence for this from our model simulations – the slope of the BNPP-MAP regression (0.24 +/- 0.03, slope estimate +/- standard error) was shallower than the slope of the ANPP-MAP regression (0.29 +/- 0.02, Fig. A8). Also, differences in functional composition of vegetation may drive site differences in root:shoot (e.g., annual versus perennial species). Despite the additional uncertainty associated with total NPP, we found that MAP was a strong predictor of total NPP across the six grassland sites (Fig. 2a).

We predicted that C residence time should be greater in (1) cooler systems due to lower soil temperatures and shorter growing seasons and (2) drier systems due to moisture limitations on microbial activity. Previous studies examining patterns of C residence time have found relationships of varying strengths with climate or latitude (Bird et al., 1996, Chen et al., 2013, Carvalhais et al., 2014, Moore et al., 2018), biome type (Zhou and Luo, 2008), soil properties (Telles et al., 2003), vegetation tissue quality (Adair et al. 2008, Bontti et al. 2009), and land use change (Sperow et al., 2016, Wu et al., 2020). Yet, there is still much uncertainty associated with trends in C residence time (Friend et al., 2014). We did not find relationships between any of the course site-level characteristics fo0und that neither MAP nor MAT were good predictors of C residence time across the six grasslands we examined (Fig. 2b). Instead, it is likely that more nuanced characteristics of sites. SBL and SBK both had particularly short C residence times, likely

19

due to strong C limitation of microbes at these sites and high abundances of fungal decomposers that efficiently break down recalcitrant C (Collins et al., 2008, Sinsabaugh et al., 2008). Additionally, intense wet-dry cycles (Fierer and Schimel, 2002), soil burial (Brandt et al., 2010), and photo-degradation (Austin and Vivanco, 2006, Parton et al., 2007) have all been shown to be important accelerators of decomposition rates in arid systems and may be contributing to the low C residence times in these grasslands. As soil C is a function of both NPP and C residence time, it makes sense that the stronger relationship of the two is the one that is best related to present C. We found that the best variable related to present C was MAP (Fig. 2), so soil C may be more sensitive to changes in precipitation versus temperature in U.S. grassland systems. This corresponds with observational studies (Saiz et al., 2012) as well as meta-analysis findings of stronger moisture than temperature effects on net ecosystem exchange (Wu et al., 2011).

4.2 Effects of soil environment versus inherent site differences on C turnover rates

C residence time is directly related to various C turnover rates within an ecosystem (Luo et al., 2017). These turnover rates can be driven by favorability of soil environments for microbial activity (Bird et al., 1996, Carvalhais et al., 2014, Stielstra et al., 2015) or by differences in soil types and microbial communities (Williams and Rice, 2007, Collins et al., 2008, Garcia-Palacios et al., 2016, Bhattacharyya et al., 2022). With our approach, we were able to model the effect of temperature and moisture on turnover rates while accounting for site-level differences in how sensitive turnover is to soil moisture and temperature (through data-assimilation estimation of Q_{10} and *mscut* parameters; Fig. A5). At four of the six grasslands, both moisture and temperature had strong effects on C turnover during the growing season (Fig. 3a,b,d,e), which corresponds to well-known moisture and temperature controls on microbial activity (Bell et al., 2008). However, in the mesic tallgrass prairie (KNZ) and the cooler shortgrass prairie (CPER), we found moisture limitation on C turnover was minimal (Fig. 3c,f). At KNZ, this was likely due to relatively high soil moisture levels throughout the growing season (Table B6). In conjunction with soil temperatures optimal for microbial activity, this resulted in high C turnover rates throughout the growing season at KNZ (Fig. 3f) and low overall ecosystem C residence times.

Alternately, soils at CPER are coarse (Table B1) and become very dry during later months of the growing season, yet C turnover was not limited within the model by soil moisture. The lack of sensitivity of C turnover to soil moisture may be due to microbial communities adjusted to low soil moisture conditions at the site. The *mscut* parameter in TECO represents the soil moisture level at which C turnover – and by inference, soil microbial activity – in the system becomes limited. Because we were able to use daily soil CO_2 fluxes that were directly linked with soil temperature and soil moisture data for at least two years at each site, our estimates of *mscut* (and Q_{10}) parameters were remarkably well constrained (Fig. A4; Table B2). The estimate of the *mscut* parameter at CPER was 7%, the lowest of all six sites. This means that when volumetric soil moisture is above 7%, microbial activity is not restricted by soil moisture in the model. Soils at CPER during the growing season (June-Sept) were the driest of all the sites, having an average soil volumetric water content (VWC) of 11% (Table B6). Additionally, the site having the second driest soils (12%

VWC – SBK) also had a low *mscut* estimate (Fig. A4). This raises the interesting possibility that ecosystems with drier soils have microbial communities adapted to low water conditions, which would result in C turnover rates persisting even in relatively xeric conditions. If it is the case that C turnover is less responsive to altered soil moisture, this could result in mismatches between responses of C inputs versus outputs under altered precipitation regimes, since NPP has been shown to be highly sensitive to precipitation in more arid ecosystems (Huxman et al., 2004, Sala et al., 2012, Maurer et al., 2020).

Turnover rates of more recalcitrant pools of soil carbon have the potential to have strong influences on ecosystem C residence times, as has been shown using a long-term cross-site decomposition experiment (Harmon et al., 2009). Turnover rates of more recalcitrant pools are represented in this study using the c_5 and c_6 parameters, which represent the amount of C lost from the slow and passive C pools each day. It is important to note that these turnover estimates represent the inherent turnover rates without the effects of moisture and temperature. The estimates for the c5 parameter were well constrained across all sites by the data assimilation process (Figure A2) and turnover rate estimates were relatively slow, ranging from 8.7 years at HPG to 21.4 years at CPER. Indeed, the turnover rate of the slow pool at CPER was a big reason why the ecosystem C residence time was high at that site (Fig. 3i). Although lignin and cellulose contents of litter have been shown to be important drivers of turnover rates of intermediate C pools (Adair et al. 2008), the CPER site is dominated by *Bouteloua gracilis*, a C_4 perennial grass that has relatively high cellulose and tissue nitrogen, and low lignin (Adair et al. 2008, Blumenthal et al., 2020). As such, we think it unlikely that litter quality is driving these slow rates. One reason the data-driven model represents slow turnover rates at CPER is that the temperature scalar is limiting turnover rates (Fig. 3c). This may be a combination of the colder temperatures and a low Q_{10} estimate at CPER. Only the HPG is cooler, yet the Q_{10} estimate at HPG is much greater than at CPER (Fig. A5, Table B2). This raises the interesting possibility that the decomposer communities at the shortgrass site may be strongly temperature limited, although additional inquiries are necessary to assess potential mechanisms. It could also be that C in CPER is older, and thus less susceptible to losses via decomposition (Conant et al., 2011). This idea fits with findings from findings of Liski et al., (1999) showing that decomposition rates of old soil C are relatively temperature insensitive, which aligns with the low Q_{10} value estimated for CPER.

The potential distribution of the c_6 parameter resulting from the data assimilation process was quite broad for each site (Fig. A2), which is likely a big part of the uncertainty present within our estimated ecosystem C residence times and the resultant uncertainty around the estimate of C capacity (grey bars in Fig. 5). For example, the MLE of the $c6$ parameter for the black grama grassland was 1.55E-05 g C · g C_s^{-1} · day^{-1} (Table B2), which translates to a baseline turnover rate of 177 years for the passive C pool. Yet, the lower bound of the 95% confidence interval for the $c6$ parameter at the same site results in a baseline turnover rate of 1940 years. Differences in passive C turnover rates can have substantial effects on ecosystem C residence times, as shown in our sensitivity analysis (Fig. 4). In terms of our example above, going from passive C turnover rates of 177 to 1940 years causes ecosystem C residence time to go from 27 to 62 years. In this example, the magnitude of

21

change of the ecosystem C residence time is less than that of the passive C turnover rates because ecosystem C residence time incorporates turnover of many other C pools, and not all C molecules end up in recalcitrant C pools. The overall effect on C saturation is substantial and important. We would like to note that variation in the passive and slow C turnover rates was a major component of the uncertainty in C capacity and saturation estimates (Fig. 5). This observation highlights the importance of these recalcitrant C pools for limiting losses of C from ecosystems.

4.3 Patterns of C saturation

Three of the grasslands we assessed had large gaps between present C and C capacity (CPER, HPG, and HAR; Fig. 5). Similar to forests acting as long-term C sinks during recovery from clear cutting regimes (Pan et al. 2011), it is possible that these cooler and/or wetter grassland ecosystems will act as C sinks due to long-term agricultural or other land-management legacies (Smith, 2014). These systems may be buffered against C losses if environmental changes occur, at least in the short-term. Alternately, the two hot and dry ecosystems showed high C saturation levels (Fig. 5), which corresponds with previous work at the SBK site showing this system is often a C source (Petrie et al., 2015), although long-term SOC data from this site indicate no net change in total soil C over time (Hou et al. 2021). High C saturation in these systems may also lead to C losses in the future, especially if global changes chronically reduce either NPP or C residence times. Short term effects on NPP or C residence times, such as those imposed by drought, may not have as strong effects on soil C because they do not permanently modify the capacity to store C of these systems, which may explain a lack of response of soil C in drought experiments (Holguin et al., 2022).

KNZ had short C residence time, but it also had the highest NPP estimate (Table 2), which should have resulted in a high C capacity. Yet, this system is burned annually in the spring, reflecting common management practices in this region (Knapp et al., 1998; Freckleton, 2004). Burning minimizes the amount of aboveground tissue that is incorporated into the soil due to volatilization of C to the atmosphere (Seastedt, 1988), although some C is deposited as pyrogenic C (Soong and Contrufo, 2015). Despite these annual losses, C capacity is still relatively close to present C, perhaps due to increased root production under frequent fire regimes (Johnson and Matchett, 2001). This may be one reason that research in this ecosystem has found that soil C is resistant to altered environmental conditions despite frequent fire (Wilcox et al., 2016), which has been predicted to reduce soil C through time due to losses through volatization (Ojima et al. 1994).

Our estimates of soil C extended from 0-20 cm in the soil, which presents two potential limitation in this study. First, since our measurements of soil C were from 0-10 cm in the soil, it was necessary to extrapolate this C to 20 cm using depth-soil C relationships from each site. This was important to match depths with all the other measurements used in this study, but the

22

520 extrapolation process introduces additional sources of error. Additionally, our estimates of both C capacity and present C did not include measurements of C below 20 cm in the soil. Deeper C represents an additional store of C in many ecosystems and may stabilize C in ecosystems where C inputs by roots at depth are frequent, such as savanna and shrubland ecosystems. Additionally, soil microbial communities differ markedly in deeper soil layers than shallow layers (Fierer et al., 2003), so turnover rates across these systems may be quite different for deeper soils. Yet in many grasslands, C fluxes aboveground

525 and in shallow soil layers are more likely to respond under global change scenarios than deeper soils because: (1) the proportion of root production of soil organic C and microbial activity are typically greatest within shallow soil layers (Jackson et al., 1996, Jobággy and Jackson, 2000, Blume et al., 2002, Taylor et al., 2002), and (2) altered air temperature is more likely to impact soil temperatures in surface soils versus deeper soils.

5 Conclusions

530 Here we used a recently developed metric, carbon capacity, to assess potential future trajectories of ecosystem C across six grasslands in the US Great Plains, and to identify grasslands that may be vulnerable to C loss under future global change scenarios. We showed that hot and dry grasslands had C contents greater than their C capacity, suggesting future C loss in these systems, especially if environmental conditions continue to change

. As arid ecosystems have been shown to be key components of the global C cycle due to their broad spatial

535 extent (Poulter et al., 2014), understanding how NPP and ecosystem carbon residence times respond to alterations in environmental conditions in these ecosystems is vital for assessing future global C budgets. Additionally, the effect of frequent burning on C saturation suggests that land management practices that remove aboveground biomass may result in reduced capacity for these systems to be C sinks into the future. However, the effects of disturbances such as fire are complex and often are critical to maintaining ecosystem structure so holistic consideration of all effects is important for

540 management decisions. Because anthropogenic and climate effects on ecosystems are global and ubiquitous, considerations of how land management and environmental impacts interact to control ecosystem functioning are critical for land management and policy decisions related to C sequestration.

Appendices:

Appendix A. Supplemental Figures A1-A8

545 Appendix B. Supplemental Tables B1-B6

Appendix C. Supplemental text describing data collection and cleaning methods

Appendix D. Model evaluation text, Table D1, Figures D1-D2

Appendix E. Land use history of study sites

550

555

560

Appendix A. Supplemental figures A1-A8
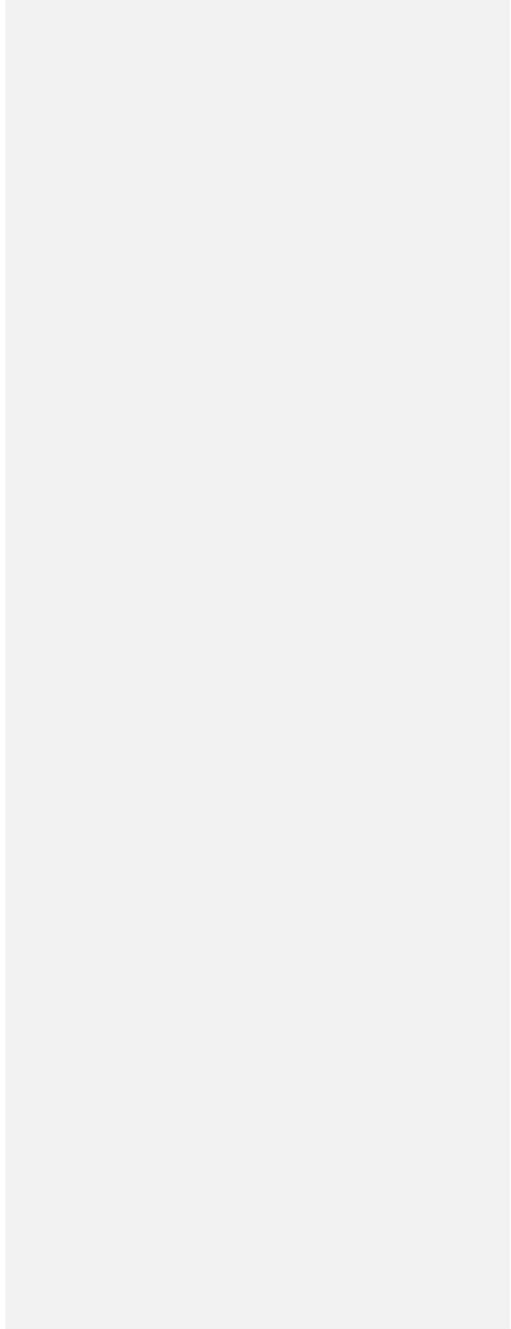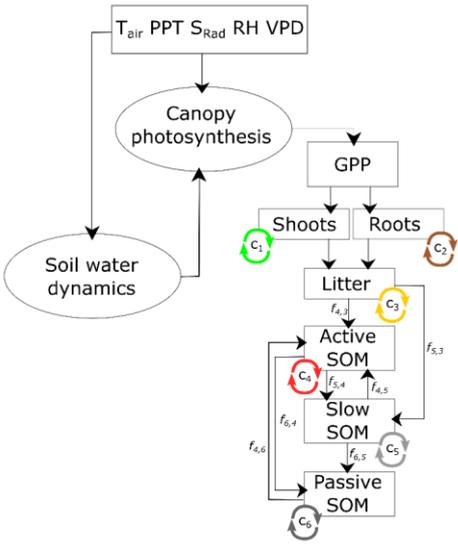
Figure A1. Schematic of the submodels making up the Terrestrial Ecosystem model. Canopy photosynthesis is determined by hourly meteorological information through direct impacts (e.g., vapor pressure deficit) and alterations to soil environmental conditions (e.g., soil moisture and temperature). GPP is estimated from the canopy photosynthesis model. Carbon from the canopy model is transferred to different components of vegetation, which is summed over an annual time step to estimate NPP (GPP – autotrophic respiration). See Weng and Luo (2008) for additional details of the model. The soil C model incorporates turnover rates for aboveground vegetation (c_1), roots (c_2), litter (c_3), active SOM (c_4), slow SOM (c_5), and passive SOM (c_6). Turnover rates are modified by an environmental scalar (τ) at each time step. The proportion of C transferred between pools are controlled by the $f_{i,j}$ parameters, which represent the proportion of C turnover transferred from C pool j to pool l, with the pool numbers corresponding to the subscripts by the C turnover parameters.
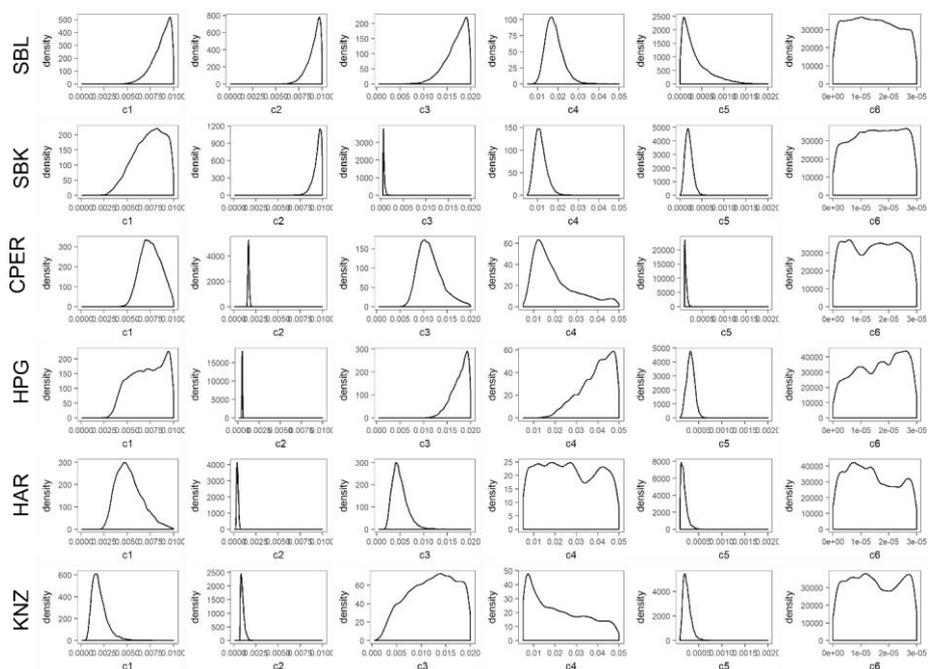
Figure A2. Density plots showing distribution of estimated carbon turnover parameters (columns) using data assimilation techniques with a 6 pool carbon model and 4-5 data sets describing carbon pools and fluxes at each of the six sites (rows). Densities reflect 4 chains of 360k simulations each, with the first 20k simulations removed. SBL= Blue grama dominated site at the Sevilleta National Wildlife Refuge; SBK= Black grama dominated site at the Sevilleta National Wildlife Refuge; CPER=central plains experimental range; HPG=High Plains Grassland Research Station; HAR=Hays Agricultural Research Station; KNZ=Konza Prairie Biological Station. All carbon turnover parameters are in units of gC lost gC^{-1} day^{-1}: c1=leaf turnover; c2=root turnover; c3=litter turnover; c4=fast SOM turnover; c5=slow SOM turnover; c6=passive SOM turnover.
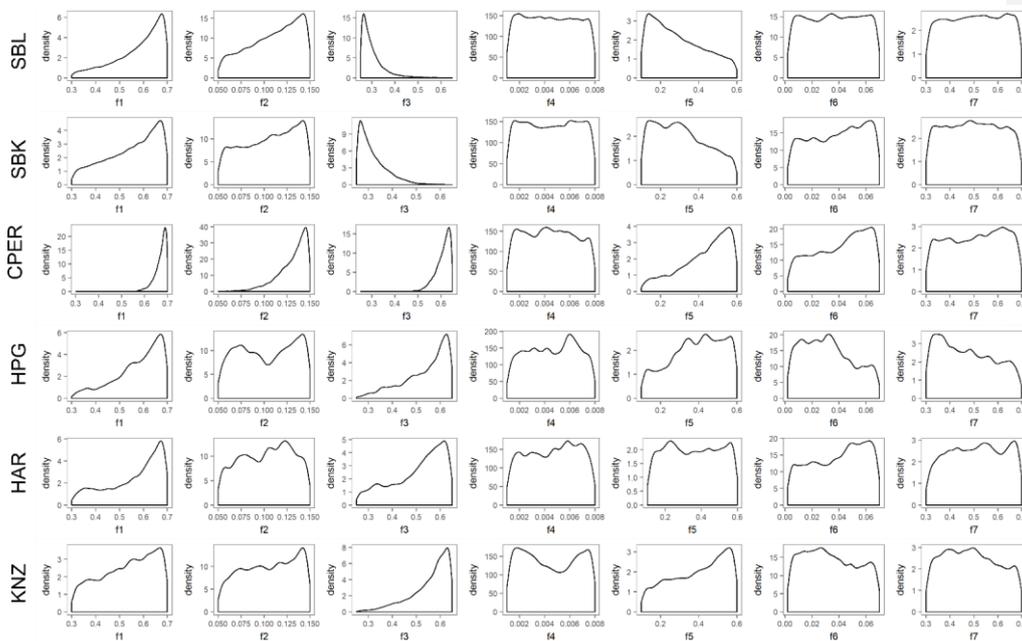
Figure A3. Density plots showing distribution of estimated carbon transfer parameters (columns) using data assimilation techniques with a 6 pool carbon model and 4-5 data sets describing carbon pools and fluxes at each of the six sites (rows). Densities reflect 4 chains of 360k simulations each, with the first 20k simulations removed. SBL= Blue grama dominated site at the Sevilleta National Wildlife Refuge; SBK= Black grama dominated site at the Sevilleta National Wildlife Refuge; CPER=central plains experimental range; HPG=High Plains Grassland Research Station; HAR=Hays Agricultural Research Station; KNZ=Konza Prairie Biological Station. Transfer parameters (fx,y) dictate the proportion of C turnover in pool y transferring to pool x: f1=f43; f2=f53; f3=f54; f4=f64; f5=f45; f6=f65; f7=f46.

Figure A4. Density plots showing distribution of environmental scaling parameters (columns) dictating decomposition rates. We used data assimilation techniques with a 6 pool carbon model and 4-5 data sets describing carbon pools and fluxes at each of the six sites (rows). Densities reflect 4 chains of 360k simulations each, with the first 20k simulations removed. SBL= Blue grama dominated site at the Sevilleta National Wildlife Refuge; SBK= Black grama dominated site at the Sevilleta National Wildlife Refuge; CPER=central plains experimental range; HPG=High Plains Grassland Research Station; HAR=Hays Agricultural Research Station; KNZ=Konza Prairie Biological Station. mscut is the soil moisture level at which decomposition rates begin to become water limited; Q10 is the temperature sensitivity of decomposition.
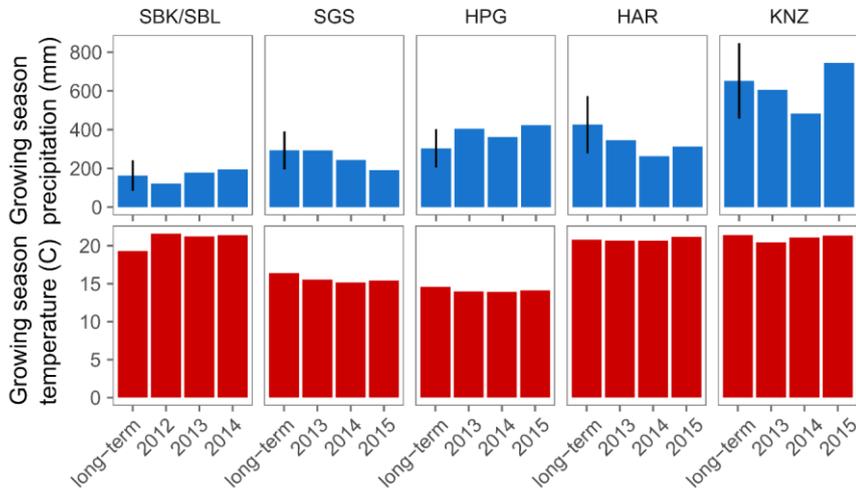
Figure A5. Precipitation and air temperature during the growing season (Apr-Oct for SBK and SBL, Apr-Sept for all other sites) during the three focal years at each site compared with the long-term mean precipitation and air temperature. Averages represent the period of 1982-2012 obtained from Knapp et al. 2015, and error bars represent 1 standard deviation from the mean.

610
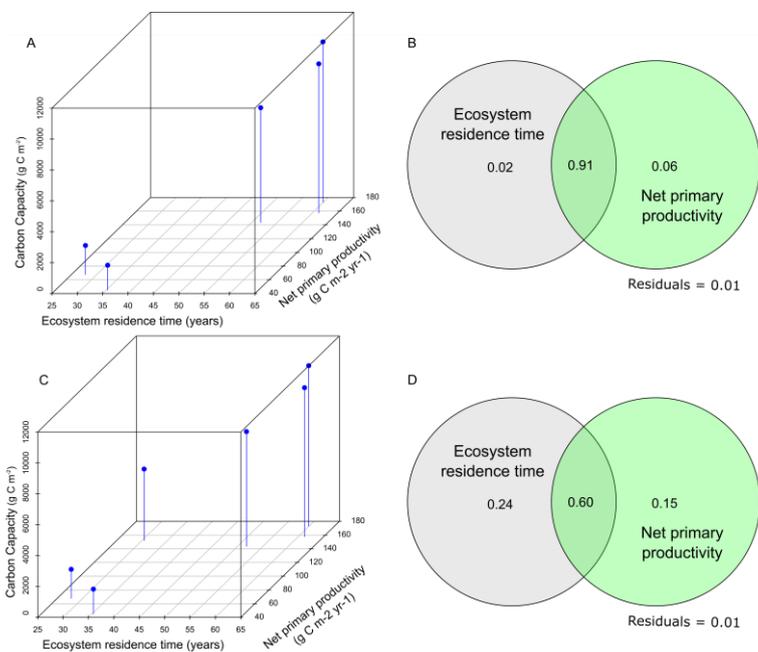
Figure A6. Three-dimensional plots (A,C) and variance partitioning results (B,D) showing the importance of ecosystem residence time and net primary productivity in making up the systems carbon capacity for our six focal ecosystems. A and B panels show results without KNZ, C and D include KNZ. In (B,D), numbers within the circles represent the amount of cross-site variance in carbon capacity explained solely by ecosystem residence time or net primary productivity. The number in the intersection represent variance explained jointly by both components.
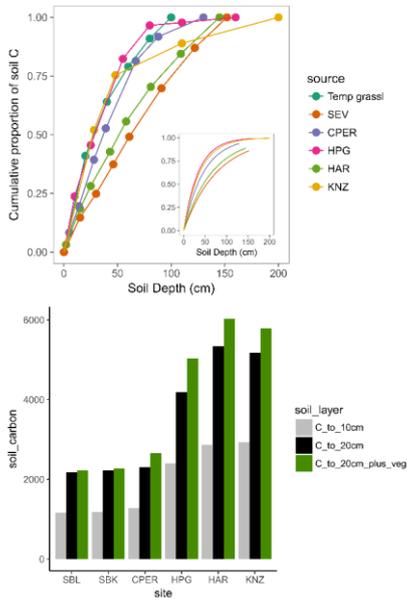
Figure A7. Top panel: Cumulative proportion of soil C along depth profile (main) and beta distribution of proportion by depth (inset). Data were obtained from the International Soil Carbon Network (see table B4) from areas close to study sites and having similar cover types and management regimes. In main panel, we included estimated proportions for temperate grasslands (Temp grass) from Jobbágy and Jackson (2000). Bottom panel: soil C measured at each study site from 0-10 cm and soil C estimates from 0-20 cm based on relationships in top panel. Estimates were obtained using: $C_{20}=C_{10}/C_{P10} \cdot C_{P20}$, where C_{10} is the soil C measured in the top 10 cm, C_{P10} is the proportion of C in the top 10 cm based on the beta regression, and C_{P20} is the proportion of C in the top 20 cm. Green bars represent soil C estimates from 0-20 cm plus vegetation C.
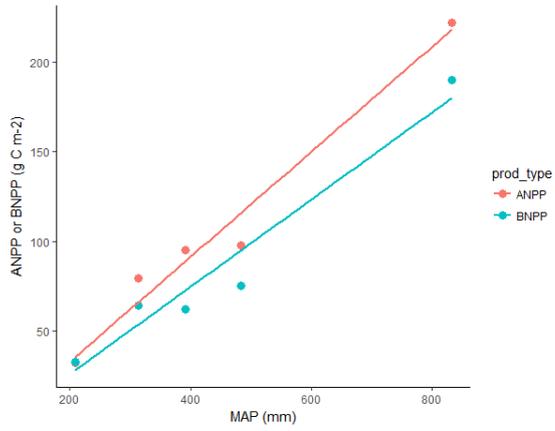
Figure A8. Average ANPP and BNPP simulation output across mean annual precipitation of our six grassland sites.

Appendix B. Supplemental tables B1-B6

Table B1. Constraints and descriptions of carbon cycling and environmental scaling parameters used in data assimilation.

Param.	Default	Lower	Upper	Description	Units
c1	1.00E-03	1.00E-04	1.00E-02	The proportion of leaf C turning over each day	gC gC-1 day-1
c2	9.00E-03	1.00E-04	1.00E-02	The proportion of root C turning over each day	gC gC-1 day-1
c3	9.00E-03	5.00E-04	2.00E-02	The proportion of litter C turning over each day	gC gC-1 day-1
c4	1.50E-02	5.00E-03	5.00E-02	Proportion of fast SOM turning over each day	gC gC-1 day-1
c5	6.00E-04	1.00E-05	2.00E-03	Proportion of slow SOM turning over each day	gC gC-1 day-1
c6	2.00E-05	1.00E-08	3.00E-05	Proportion of passive SOM turning over each day	gC gC-1 day-1
f43	2.50E-01	3.00E-01	7.00E-01	Proportion of litter C turnover going to fast SOM pool	-
f53	1.00E-01	5.00E-02	1.50E-01	Proportion of litter C turnover going to slow SOM pool	-
f54	5.00E-01	2.50E-01	6.50E-01	Proportion of fast SOM turnover going to slow SOM pool	-
f64	4.00E-03	1.00E-03	8.00E-03	Proportion of litter C turnover going to passive SOM pool	-
f45	4.20E-01	1.00E-01	6.00E-01	Proportion of slow SOM turnover going to fast SOM pool	-
f65	5.00E-02	2.00E-03	7.00E-02	Proportion of slow C turnover going to passive SOM pool	-
f46	4.50E-01	3.00E-01	7.00E-01	Proportion of passive C turnover going to fast SOM pool	-
Q10	2.20E+00	1.00E+00	4.00E+00	Temperature sensitivity of decomposition	-
mscut	2.00E-01	1.00E-02	4.00E-01	Soil moisture level at which decomposition starts to become water limited	-

33

Table B2. C cycling and environmental scaling parameters estimated via data assimilation with a six pool C model and 4-5 C pool and flux data sets for each of six grassland sites. 95% confidence intervals (CLl and cLu) are estimated from normal, log-normal, or Weibull distributions depending on the magnitude and direction of skew. Gelman-Rubin statistics (G-R) indicate convergence among independent chains.

	SBL				SBK			
Param	MLE	CLl	cLu	G-R	MLE	CLl	cLu	G-R
c1	0.009107	6.75E-03	1.00E-02	1.0	0.007977	0.004471	0.009999	1.0
c2	0.009405	7.70E-03	1.00E-02	1.0	0.00963	0.008492	0.01	1.0
c3	0.017967	1.24E-02	2.00E-02	1.0	0.00068	0.0005	0.001112	1.0
c4	0.017657	1.06E-02	2.67E-02	1.0	0.01101	0.006237	0.0172	1.0
c5	0.000232	1.00E-05	1.02E-03	1.0	0.000188	5.61E-05	0.000374	1.0
c6	1.46E-05	8.02E-07	2.87E-05	1.0	1.55E-05	1.41E-06	2.93E-05	1.0
f43	0.618122	3.74E-01	7.00E-01	1.0	0.593098	0.347119	0.699949	1.0
f53	0.110032	6.02E-02	1.50E-01	1.0	0.1055	0.056978	0.149515	1.0
f54	0.298433	2.50E-01	4.10E-01	1.0	0.312915	0.250004	0.435435	1.0
f64	0.004441	1.16E-03	7.71E-03	1.0	0.004506	0.001239	0.007792	1.0
f45	0.262651	1.00E-01	5.45E-01	1.0	0.31254	0.103977	0.552567	1.0
f65	0.036233	4.11E-03	6.77E-02	1.0	0.038417	0.005276	0.068779	1.0
f46	0.504545	3.17E-01	6.90E-01	1.0	0.497965	0.312594	0.681608	1.0
mscut	0.223073	1.78E-01	2.56E-01	1.0	0.159795	0.135553	0.18398	1.0
Q10	1.895981	1.07E+00	2.76E+00	1.0	1.597074	1.231482	1.986987	1.0

	CPER				HPG			
Param	MLE	CLl	cLu	G-R	MLE	CLl	cLu	G-R
c1	0.00746	0.005609	0.00966	1.0	0.007872	0.004192	0.009959	1.1
c2	0.001675	0.001518	0.00184	1.0	0.000488	0.000417	0.000562	1.0
c3	0.011091	0.006979	0.016717	1.0	0.018395	0.0143	0.019997	1.0
c4	0.017479	0.006234	0.041909	1.0	0.042184	0.024925	0.049978	1.1
c5	0.000128	0.0001	0.000181	1.0	0.000314	0.000164	0.000482	1.0
c6	1.49E-05	7.57E-07	2.86E-05	1.1	1.64E-05	1.97E-06	2.92E-05	1.2
f43	0.68024	0.618193	0.699996	1.0	0.576301	0.377749	0.699959	1.1
f53	0.137347	0.099531	0.149997	1.0	0.102849	0.057045	0.14747	1.3
f54	0.62252	0.546666	0.649987	1.0	0.574702	0.35944	0.649937	1.1
f64	0.004421	0.001187	0.007682	1.1	0.004583	0.001361	0.00768	1.2
f45	0.427899	0.176967	0.599756	1.0	0.388533	0.150328	0.587869	1.2
f65	0.040839	0.007248	0.069772	1.1	0.032149	0.002948	0.060738	1.1
f46	0.506596	0.316463	0.687456	1.0	0.473907	0.305835	0.667426	1.2
mscut	0.073406	0.014973	0.125796	1.0	0.231396	0.205847	0.253547	1.0
Q10	1.248167	1.10994	1.393126	1.0	3.482896	2.773369	3.950379	1.0

Param	HAR				KNZ			
	MLE	CLl	cLu	G-R	MLE	CLl	cLu	G-R
c1	0.005025	0.002799	0.007883	1.0	0.001854	0.000722	0.00367	1.0
c2	0.000414	0.000257	0.0006	1.0	0.000967	0.000699	0.001413	1.0
c3	0.004664	0.002313	0.007928	1.0	0.013651	0.004197	0.019902	1.0
c4	0.026455	0.006518	0.047266	1.0	0.021989	0.005002	0.045437	1.0
c5	0.000171	0.0001	0.000308	1.0	0.000233	0.000106	0.00041	1.0
c6	1.41E-05	9.88E-07	2.88E-05	1.0	1.50E-05	1.46E-06	2.94E-05	1.0
f43	0.561531	0.34928	0.699978	1.0	0.531489	0.347243	0.696558	1.1
f53	0.102973	0.057002	0.146251	1.1	0.104992	0.05725	0.148682	1.1
f54	0.54796	0.303471	0.649941	1.3	0.586921	0.387489	0.649992	1.0
f64	0.004599	0.001247	0.007561	1.2	0.004439	0.001255	0.007846	1.0
f45	0.354072	0.125197	0.577835	1.3	0.39581	0.156163	0.599482	1.1
f65	0.03924	0.006196	0.069346	1.1	0.034188	0.004299	0.066817	1.1
f46	0.509573	0.327535	0.691565	1.0	0.490831	0.314648	0.683017	1.1
mscut	0.283857	0.231203	0.328458	1.0	0.114386	0.013291	0.232586	1.1
Q10	2.503186	1.929534	3.128982	1.0	3.445054	2.277028	3.999685	1.0

Table B3. Cross correlations between Markov Chain Monte Carlo output of different model parameters during data assimilation.

site	param	c1	c2	c3	c4	c5	c6	f43	f53	f54	f64	f45	f65	f46	mscut	Q10
SBL	c1	1	0.06	0.05	0.14	0.11	0.02	-0.04	-0.04	0.04	0.01	-0.02	0.02	-0.01	-0.09	-0.17
SBL	c2	0.06	1	0.04	0.13	0.02	0	-0.04	-0.02	0	0	0.01	0.01	0	0.05	-0.07
SBL	c3	0.05	0.04	1	0.1	-0.02	0.03	0.11	-0.01	-0.02	0.01	0.01	0.01	-0.02	0.01	-0.07
SBL	c4	0.14	0.13	0.1	1	0.47	0.02	0	-0.05	0.17	0.02	-0.05	0.02	-0.01	-0.18	-0.43
SBL	c5	0.11	0.02	-0.02	0.47	1	-0.03	-0.03	0.02	0.41	0.03	-0.21	0.06	0	-0.79	-0.86
SBL	c6	0.02	0	0.03	0.02	-0.03	1	0.01	-0.01	0	0.05	-0.02	-0.02	-0.05	0.02	0
SBL	f43	-0.04	-0.04	0.11	0	-0.03	0.01	1	0.01	-0.01	-0.02	0.04	0	-0.04	0.1	0.18
SBL	f53	-0.04	-0.02	-0.01	-0.05	0.02	-0.01	0.01	1	0.01	0	-0.04	0	0.01	0.04	0.09
SBL	f54	0.04	0	-0.02	0.17	0.41	0	-0.01	0.01	1	-0.03	-0.08	-0.01	0.03	-0.22	-0.21
SBL	f64	0.01	0	0.01	0.02	0.03	0.05	-0.02	0	-0.03	1	-0.04	-0.01	0	-0.04	-0.04
SBL	f45	-0.02	0.01	0.01	-0.05	-0.21	-0.02	0.04	-0.04	-0.08	-0.04	1	-0.03	0.03	0.25	0.28
SBL	f65	0.02	0.01	0.01	0.02	0.06	-0.02	0	0	-0.01	-0.01	-0.03	1	0.02	-0.03	-0.02
SBL	f46	-0.01	0	-0.02	-0.01	0	-0.05	-0.04	0.01	0.03	0	0.03	0.02	1	0.01	0.01
SBL	mscut	-0.09	0.05	0.01	-0.18	-0.79	0.02	0.1	0.04	-0.22	-0.04	0.25	-0.03	0.01	1	0.87
SBL	Q10	-0.17	-0.07	-0.07	-0.43	-0.86	0	0.18	0.09	-0.21	-0.04	0.28	-0.02	0.01	0.87	1
SBK	c1	1.00	0.05	0.01	0.09	0.11	0.01	0.03	0.03	0.02	0.04	-0.01	-0.02	0.04	0.00	-0.16
SBK	c2	0.05	1.00	0.05	0.15	0.17	-0.01	-0.01	0.00	0.02	0.01	-0.01	0.00	0.01	0.07	-0.21
SBK	c3	0.01	0.05	1.00	0.05	-0.17	0.01	0.08	0.06	0.01	0.00	0.01	-0.02	0.00	0.05	-0.16
SBK	c4	0.09	0.15	0.05	1.00	0.52	-0.01	0.00	-0.02	0.06	-0.01	0.04	0.02	0.02	-0.01	-0.44
SBK	c5	0.11	0.17	-0.17	0.52	1.00	-0.07	0.09	0.01	0.27	0.01	0.11	0.06	0.01	-0.31	-0.75
SBK	c6	0.01	-0.01	0.01	-0.01	-0.07	1.00	0.04	0.04	-0.02	-0.06	-0.05	-0.01	0.03	-0.02	0.00
SBK	f43	0.03	-0.01	0.08	0.00	0.09	0.04	1.00	-0.05	0.09	0.00	0.01	-0.08	0.06	-0.02	0.00
SBK	f53	0.03	0.00	0.06	-0.02	0.01	0.04	-0.05	1.00	0.02	0.04	0.04	-0.08	-0.10	0.00	0.02
SBK	f54	0.02	0.02	0.01	0.06	0.27	-0.02	0.09	0.02	1.00	-0.02	0.02	-0.03	0.01	0.03	-0.02
SBK	f64	0.04	0.01	0.00	-0.01	0.01	-0.06	0.00	0.04	-0.02	1.00	-0.02	-0.01	0.00	-0.01	-0.01
SBK	f45	-0.01	-0.01	0.01	0.04	0.11	-0.05	0.01	0.04	0.02	-0.02	1.00	-0.06	0.00	0.06	0.07
SBK	f65	-0.02	0.00	-0.02	0.02	0.06	-0.01	-0.08	-0.08	-0.03	-0.01	-0.06	1.00	0.01	-0.01	-0.02
SBK	f46	0.04	0.01	0.00	0.02	0.01	0.03	0.06	-0.10	0.01	0.00	0.00	0.01	1.00	0.00	-0.01
SBK	mscut	0.00	0.07	0.05	-0.01	-0.31	-0.02	-0.02	0.00	0.03	-0.01	0.06	-0.01	0.00	1.00	0.53
SBK	Q10	-0.16	-0.21	-0.16	-0.44	-0.75	0.00	0.00	0.02	-0.02	-0.01	0.07	-0.02	-0.01	0.53	1.00
CPER	c1	1.00	0.18	-0.05	-0.08	0.02	0.04	-0.01	0.04	0.05	0.01	0.02	0.02	-0.02	0.17	-0.16

36

CPER	c2	0.18	1.00	0.09	0.00	0.06	0.02	-0.02	-0.03	-0.03	0.01	-0.02	-0.02	0.00	0.50	-0.47
CPER	c3	-0.05	0.09	1.00	-0.30	-0.01	0.07	0.08	0.02	-0.06	-0.07	-0.05	-0.04	0.00	0.08	-0.02
CPER	c4	-0.08	0.00	-0.30	1.00	0.01	-0.04	-0.03	-0.09	0.08	0.06	0.00	0.01	0.10	-0.03	0.01
CPER	c5	0.02	0.06	-0.01	0.01	1.00	-0.02	0.09	0.09	0.17	0.00	0.18	0.05	-0.03	0.03	-0.13
CPER	c6	0.04	0.02	0.07	-0.04	-0.02	1.00	0.03	0.05	0.05	0.02	-0.04	0.05	0.03	0.00	-0.02
CPER	f43	-0.01	-0.02	0.08	-0.03	0.09	0.03	1.00	-0.08	-0.11	0.03	-0.06	-0.02	-0.02	-0.02	0.08
CPER	f53	0.04	-0.03	0.02	-0.09	0.09	0.05	-0.08	1.00	-0.16	-0.13	-0.03	0.05	-0.04	-0.03	0.06
CPER	f54	0.05	-0.03	-0.06	0.08	0.17	0.05	-0.11	-0.16	1.00	0.01	-0.05	-0.05	0.01	-0.03	0.10
CPER	f64	0.01	0.01	-0.07	0.06	0.00	0.02	0.03	-0.13	0.01	1.00	-0.02	0.01	-0.03	0.01	0.00
CPER	f45	0.02	-0.02	-0.05	0.00	0.18	-0.04	-0.06	-0.03	-0.05	-0.02	1.00	0.01	-0.11	-0.01	0.07
CPER	f65	0.02	-0.02	-0.04	0.01	0.05	0.05	-0.02	0.05	-0.05	0.01	0.01	1.00	0.02	-0.03	0.01
CPER	f46 msc	-0.02	0.00	0.00	0.10	-0.03	0.03	-0.02	-0.04	0.01	-0.03	-0.11	0.02	1.00	0.01	-0.01
CPER	ut	0.17	0.50	0.08	-0.03	0.03	0.00	-0.02	-0.03	-0.03	0.01	-0.01	-0.03	0.01	1.00	-0.03
CPER	Q10	-0.16	-0.47	-0.02	0.01	-0.13	-0.02	0.08	0.06	0.10	0.00	0.07	0.01	-0.01	-0.03	1.00
HPG	c1	1.00	-0.11	0.21	0.16	-0.10	-0.04	0.03	-0.07	-0.22	0.13	-0.17	-0.01	-0.08	-0.09	0.01
HPG	c2	-0.11	1.00	0.04	-0.04	0.46	-0.01	0.06	0.08	0.11	-0.06	0.02	-0.07	0.02	0.46	-0.44
HPG	c3	0.21	0.04	1.00	-0.07	-0.06	-0.02	-0.12	-0.13	-0.14	0.05	-0.01	0.00	-0.11	0.01	-0.03
HPG	c4	0.16	-0.04	-0.07	1.00	-0.07	-0.14	-0.13	0.02	-0.05	-0.01	-0.05	0.14	0.04	0.02	0.06
HPG	c5	-0.10	0.46	-0.06	-0.07	1.00	0.04	0.43	0.16	0.57	0.05	0.39	-0.10	0.12	0.02	-0.47
HPG	c6	-0.04	-0.01	-0.02	-0.14	0.04	1.00	0.21	0.05	0.14	0.12	0.03	-0.12	0.11	0.04	0.05
HPG	f43	0.03	0.06	-0.12	-0.13	0.43	0.21	1.00	0.05	0.17	-0.03	0.06	-0.17	0.11	0.04	-0.01
HPG	f53	-0.07	0.08	-0.13	0.02	0.16	0.05	0.05	1.00	0.01	-0.13	-0.13	-0.09	0.14	-0.02	-0.11
HPG	f54	-0.22	0.11	-0.14	-0.05	0.57	0.14	0.17	0.01	1.00	0.06	0.08	-0.17	0.11	0.11	-0.01
HPG	f64	0.13	-0.06	0.05	-0.01	0.05	0.12	-0.03	-0.13	0.06	1.00	0.15	0.02	0.00	-0.02	0.04
HPG	f45	-0.17	0.02	-0.01	-0.05	0.39	0.03	0.06	-0.13	0.08	0.15	1.00	-0.02	0.01	-0.04	-0.06
HPG	f65	-0.01	-0.07	0.00	0.14	-0.10	-0.12	-0.17	-0.09	-0.17	0.02	-0.02	1.00	-0.11	0.00	0.07
HPG	f46 msc	-0.08	0.02	-0.11	0.04	0.12	0.11	0.11	0.14	0.11	0.00	0.01	-0.11	1.00	0.01	-0.01
HPG	ut	-0.09	0.46	0.01	0.02	0.02	0.04	0.04	-0.02	0.11	-0.02	-0.04	0.00	0.01	1.00	0.54
HPG	Q10	0.01	-0.44	-0.03	0.06	-0.47	0.05	-0.01	-0.11	-0.01	0.04	-0.06	0.07	-0.01	0.54	1.00
HAR	c1	1.00	0.86	0.55	0.04	0.45	0.10	-0.03	-0.10	-0.24	0.00	0.00	-0.06	0.00	0.66	-0.45
HAR	c2	0.86	1.00	0.63	0.03	0.51	0.08	-0.10	-0.10	-0.29	0.00	0.00	-0.07	0.03	0.76	-0.48
HAR	c3	0.55	0.63	1.00	0.02	0.32	0.01	-0.01	-0.06	-0.13	0.00	0.05	-0.08	0.03	0.48	-0.33
HAR	c4	0.04	0.03	0.02	1.00	-0.01	-0.06	-0.18	-0.02	0.15	0.05	-0.13	0.11	0.08	0.03	0.01
HAR	c5	0.45	0.51	0.32	-0.01	1.00	0.03	0.25	-0.10	0.23	0.04	0.23	-0.04	-0.03	0.31	-0.36
HAR	c6	0.10	0.08	0.01	-0.06	0.03	1.00	0.12	0.01	-0.06	-0.06	0.01	-0.05	-0.28	0.02	-0.13
HAR	f43	-0.03	-0.10	-0.01	-0.18	0.25	0.12	1.00	-0.30	-0.01	0.09	0.13	-0.10	-0.21	-0.12	0.03

37

HAR	f53	-0.10	-0.10	-0.06	-0.02	-0.10	0.01	-0.30	1.00	-0.06	-0.12	-0.02	-0.01	-0.06	-0.03	0.12
HAR	f54	-0.24	-0.29	-0.13	0.15	0.23	-0.06	-0.01	-0.06	1.00	-0.05	-0.11	0.03	-0.01	-0.16	0.28
HAR	f64	0.00	0.00	0.00	0.05	0.04	-0.06	0.09	-0.12	-0.05	1.00	0.08	0.17	-0.04	-0.02	-0.02
HAR	f45	0.00	0.00	0.05	-0.13	0.23	0.01	0.13	-0.02	-0.11	0.08	1.00	-0.12	0.04	-0.01	0.00
HAR	f65	-0.06	-0.07	-0.08	0.11	-0.04	-0.05	-0.10	-0.01	0.03	0.17	-0.12	1.00	-0.10	-0.06	0.01
HAR	f46	0.00	0.03	0.03	0.08	-0.03	-0.28	-0.21	-0.06	-0.01	-0.04	0.04	-0.10	1.00	0.03	-0.02
HAR	msc ut	0.66	0.76	0.48	0.03	0.31	0.02	-0.12	-0.03	-0.16	-0.02	-0.01	-0.06	0.03	1.00	0.12
HAR	Q10	-0.45	-0.48	-0.33	0.01	-0.36	-0.13	0.03	0.12	0.28	-0.02	0.00	0.01	-0.02	0.12	1.00
KNZ	c1	1.00	0.52	0.04	-0.07	0.28	-0.07	-0.03	0.00	-0.07	-0.02	0.02	0.03	0.01	0.04	-0.48
KNZ	c2	0.52	1.00	0.01	-0.13	0.55	-0.05	-0.07	-0.02	-0.10	-0.06	0.03	0.04	0.02	0.08	-0.93
KNZ	c3	0.04	0.01	1.00	-0.05	0.08	0.09	0.10	0.04	0.02	-0.12	0.03	0.01	0.05	0.04	-0.01
KNZ	c4	-0.07	-0.13	-0.05	1.00	-0.21	-0.02	-0.05	0.11	0.03	0.08	-0.12	-0.04	-0.07	-0.09	0.11
KNZ	c5	0.28	0.55	0.08	-0.21	1.00	-0.05	0.19	0.08	0.23	-0.02	0.34	0.13	0.03	0.17	-0.48
KNZ	c6	-0.07	-0.05	0.09	-0.02	-0.05	1.00	0.02	0.06	0.12	-0.10	0.02	-0.08	-0.03	-0.02	0.03
KNZ	f43	-0.03	-0.07	0.10	-0.05	0.19	0.02	1.00	-0.02	0.05	0.10	0.01	0.01	-0.01	-0.04	0.07
KNZ	f53	0.00	-0.02	0.04	0.11	0.08	0.06	-0.02	1.00	0.05	0.09	0.05	-0.13	-0.12	0.04	0.04
KNZ	f54	-0.07	-0.10	0.02	0.03	0.23	0.12	0.05	0.05	1.00	0.00	-0.12	-0.02	-0.05	-0.02	0.09
KNZ	f64	-0.02	-0.06	-0.12	0.08	-0.02	-0.10	0.10	0.09	0.00	1.00	-0.14	0.07	-0.11	0.05	0.06
KNZ	f45	0.02	0.03	0.03	-0.12	0.34	0.02	0.01	0.05	-0.12	-0.14	1.00	0.08	0.14	0.09	-0.02
KNZ	f65	0.03	0.04	0.01	-0.04	0.13	-0.08	0.01	-0.13	-0.02	0.07	0.08	1.00	0.00	-0.07	-0.06
KNZ	f46	0.01	0.02	0.05	-0.07	0.03	-0.03	-0.01	-0.12	-0.05	-0.11	0.14	0.00	1.00	0.01	-0.02
KNZ	msc ut	0.04	0.08	0.04	-0.09	0.17	-0.02	-0.04	0.04	-0.02	0.05	0.09	-0.07	0.01	1.00	0.16
KNZ	Q10	-0.48	-0.93	-0.01	0.11	-0.48	0.03	0.07	0.04	0.09	0.06	-0.02	-0.06	-0.02	0.16	1.00

690

695

700

38

Table B4. Descriptions of soil profile data sets obtained from the International Soil Carbon Network

Location	Site code	Latitude	Longitude	Profile depth (cm)
Sevilleta National Wildlife Refuge, New Mexico	81NM053005	34.18703	-107.21	152
Central Plains Experimental Range, Colorado	S1991CO123007	40.82806	-104.786	130
Cheyenne, Wyoming	S1989WY021007	41.20889	-104.931	160
Hays, Kansas	S1968KS051001	39.01528	-99.1258	145
Konza Priarie Biological Station, Kansas	KZP 1D	39.07597	-96.5638	200

Table B5. Variance partitioning results comparing among site variation in net primary productivity explained by site-level estimates of average annual precipitation, average annual temperature, soil bulk density, grass:forb, C3:C4, and annual species abundance.

Variable 1	Variable2	Test	AdjR2	Fval	Pval
NPP	MAP				
		X1|X2	1.17	123.71	0.01
	MAP	X1X2 colin.	-0.21	NA	NA
		X2|X1	0.00	0.58	0.51
		X1+X2	0.96	63.84	<0.01
		X1|X2	0.36	32.70	0.01
	Bulk Density	X1X2 colin.	0.61	NA	NA
		X2|X1	-0.01	0.03	0.84
		X1+X2	0.95	53.74	0.02
		X1|X2	0.09	11.44	0.05
	Grass:forb	X1X2 colin.	0.87	NA	NA
		X2|X1	0.00	0.82	0.43
		X1+X2	0.96	68.27	<0.01
		X1|X2	1.15	103.19	<0.01
	C3:C4	X1X2 colin.	-0.18	NA	NA
		X2|X1	-0.01	0.04	0.83
		X1+X2	0.95	54.02	0.01
		X1|X2	0.50	74.70	0.01
	Annual species abundance	X1X2 colin.	0.47	NA	NA
		X2|X1	0.01	2.06	0.24
		X1+X2	0.97	90.77	<0.01
Eco$_{RT}$	MAT				
		X1|X2	0.54 ~~0.73~~	4.10 ~~6.57~~	0.18 ~~0.11~~
	MAP	X1X2 colin.	-0.16 ~~-0.14~~	NA ~~NA~~	NA ~~NA~~
		X2|X1	-0.09 ~~-0.11~~	0.10 ~~0.13~~	0.71 ~~0.69~~
		X1+X2	0.70 ~~0.52~~	2.05 ~~3.29~~	0.33 ~~0.14~~
		X1|X2	0.22 ~~0.35~~	2.21 ~~3.60~~	0.22 ~~0.18~~
	Bulk Density	X1X2 colin.	-0.18 ~~0.24~~	NA ~~NA~~	NA ~~NA~~
		X2|X1	0.24 ~~0.13~~	0.02 ~~0.02~~	0.86 ~~0.90~~
		X1+X2	0.72 ~~0.54~~	1.97 ~~3.12~~	0.37 ~~0.22~~
	Grass:forb	X1|X2	0.60 ~~0.81~~	4.74 ~~8.46~~	0.16 ~~0.04~~
		X1X2 colin.	-0.10 ~~0.22~~	NA ~~NA~~	NA ~~NA~~

40

	X2|X1	-0.15-0.03	0.380.75	0.520.31
	X1+X2	0.640.44	2.384.24	0.240.15
C3:C4	X1|X2	0.220.55	2.225.34	0.230.14
	X1X2 colin.	-0.180.04	NANA	NANA
	X2|X1	0.23-0.10	0.010.23	0.950.69
	X1+X2	0.730.51	1.953.44	0.250.12
Annual species abundance	X1|X2	0.360.58	3.165.31	0.220.13
	X1X2 colin.	-0.120.01	NANA	NANA
	X2|X1	0.10-0.13	0.290.03	0.690.94
	X1+X2	0.660.54	2.273.13	0.300.24

730

735

740

745

Table B6. Average soil moisture and soil temperature during June-September at our six focal grassland sites.

Site	Volumetric soil moisture (%)	Soil temperature (°C)
SBL	13.3	26.3
SBK	11.9	27.6
CPER	11.4	22.9
HPG	15.4	21.1
HAR	21.0	24.6
KNZ	20.9	24.0

755

760

Appendix C. Detailed description of data collection and cleaning methods

C1 Aboveground net primary productivity (ANPP)

At CPER, HPG, HAR, and KNZ, ANPP was collected annually by clipping two 0.1 m^2 subplots per replicate in September, sorted to remove previous years' growth, dried at 60 C for 48 hours, and weighed. At SBK and SBL, ANPP was estimated using species-specific allometric methods (Muldavin et al. 2008, Rudgers et al. 2019) within four 1 m^2 subplots within each of the 10 control plots.

C2 Vegetative litter

Litter estimates were obtained by collecting previous year's biomass to ground level in the same subplots as ANPP. Litter was not present at SBL or SBK due to rapid decomposition at the soil surface at these sites, nor at KNZ due to annual burning.

C3 Belowground net primary productivity (BNPP) and root standing crop

BNPP was estimated from 0-20 cm at each site using two root ingrowth cores per plot (Persson 1980). Ingrowth cores were constructed from 2 mm fiberglass screen molded into a 5 cm diameter 22 cm long cylinder (2 cm was left above soil surface). In April-May, a soil auger was used to drill 20 cm deep in the soil. Ingrowth cores were then inserted, filled with sieved, root free soil from the site, and packed to approximate soil density. Ingrowth cores were removed in late September and stored at 4 C until processing. Samples were elutriated to separate root biomass from soil. Samples were sorted to remove soil organic matter, dried at 60 C for 48 hours, and weighed. Finally, samples were fired at 450 C and resulting ash subtracted from the biomass value to generate an ash free estimate of BNPP. 5 cm root standing crop samples were also taken from 0-20 cm in two subplots. Standing crop root samples were processed similarly to BNPP samples, with the exception that dead roots were sorted out of the samples at the same time as SOM.

790 **C4 Soil CO$_2$ efflux**

Surface soil respiration was calculated using measurements of soil CO$_2$ concentrations (GMP 220 series probes, Vaisala Corp., Helsinki, Finland) in three replicates per site at 5, 10, and 20 cm depths, combined with diffusion rates calculated using soil temperature and moisture data collected simultaneously with CO$_2$ concentration. See Vargas & Allen (2008), and Vargas et al. (2010) for more information about calculating soil respiration rates using this method. We averaged 15 minute
795 soil respiration measurements between 10:00 am and 2:00 pm to obtain daily soil respiration values.

C5 Soil moisture and temperature

Volumetric soil moisture integrated from 0-15 cm was measured in all 10 plots every 15 minutes using time domain reflectometry probes (CS-616 model, Campbell Scientific, Inc., Logan, UT, USA). Soil temperature was measured in 3 plots at 5 cm and 10 cm depths using thermocouples (K-type, OMEGA Engineering Inc., Stamford, CT, USA).

800 **C6 Soil bulk density**

Bulk density was measured at each site from ten 7 cm diameter soil cores taken 0-30 cm. Soil cores were extracted in segments to reduce compaction. All aboveground vegetation was removed, and cores were dried at 105 C for 48 hours, then weighed. Bulk density was then calculated as:

$$BD = \frac{M_{dry}}{\pi r^2 x\, D} \tag{C1}$$

805 Where M_{dry} is the dry mass, r is the radius, and D is the depth of the soil core.

C7 Meteorological data

Hourly air temperature, precipitation, relative humidity, vapor pressure deficit (VPD), and incident photosynthetically active radiation data were obtained from nearby weather stations to run the terrestrial ecosystem model (TECO; Weng and Luo, 2008). Gaps of < 10 time steps (hours) were filled by splining, and all splined sections examined to ensure values were
810 within reasonable bounds. Gaps of longer time steps were filled from next closest meteorological stations of the same elevation. When unavailable, we calculated VPD as actual vapor pressure (e_a) minus saturation vapor pressure (e_s). e_a is estimated as:

$$e_a = \frac{RH}{100} e_s \tag{C2}$$

where RH is relative humidity, and e_s is estimated as:

44

815 $$e_s = 0.6108e^{\frac{17.27t}{t+237.3}}$$ (C3)

where t is air temperature.

C8 Soil total organic carbon

At CPER, HGR, HAR, and KNZ, percent C was measured in three 2 cm diameter 10 cm deep soil cores per plot.
Subsamples were aggregated, sieved with a 2 mm soil sieve to remove root material, dried, and ground. Samples were then
820 measured for total C via dry combustion and grass chromatography using a LECO CN 2000 combustion analyzer (LECO
Corp., Saint Joseph, MI, USA). For SBL and SBK, percent organic matter was estimated in soil from 0-10 cm depths from
nearby areas having similar soils and vegetation to the EDGE sites. Organic matter values were then converted to percent C
by dividing the percent organic matter by 1.72 (assumes 58% C stoichiometry of organic matter). Percent C for all sites was
then converted to total C using:

825 $$C_T = D \; x \; BD \; x \; C_p x \; 10000$$ (C4)

Where C_T is total carbon, D is the depth in cm to which the sample was collected, BD is the bulk density in g per cm^{-2}, and
C_p is the proportion of carbon.

C9 Plant species abundance

Abundance of plant species was estimated visually in June and August in four 1 x 1 m^2 subplots per plot to the nearest
830 percent. Species having less than 1% cover were rounded up to 1%. Calibrations of visual estimates were performed across
researchers and with measurements seasonally. Maximum cover of each species was taken for each subplot, then all
abundances were averaged across subplots to get plot-level estimates.

835

840

845

Appendix D. Model evaluation text, Table D1, Figures D1-D3

Model validation exercises were conducted to compare the ability of the model to represent (1) average plant growth across sites and (2) variability of plant growth across years within each site. To this end, models were parameterized for each site based on soil texture, field capacity, wilting point, latitude, and root:shoot ratios. Additionally, maximum and minimum
850 specific leaf area and Vcmax parameters were adjusted to better match measured above and belowground plant growth. Table 1 shows the parameter sets used for each site.

Empirical observations of ANPP and BNPP (n=10) were compared to leaf+stem biomass and root productivity from the model at the time of data collection. At CPER, HPG, HAR, and KNZ, ANPP was collected annually by clipping two 0.1 m2 subplots per replicate in September, sorted to remove previous years' growth (leaf litter), dried at 60 C for 48 hours, and
855 weighed. At SBK and SBL, ANPP was estimated using species-specific allometric methods (Muldavin et al. 2008) within four 1m2 subplots within each of the 10 replicates. BNPP within each replicate at each site was estimated from 0-20 cm using two 20 cm x 5 cm diameter root ingrowth cores per plot (Persson 1980). See Appendix 3 for additional details about empirical data collection.

Models were spun up for 500 years using cycled meteorological data from each site – all carbon pools stabilized after 200-
860 400 years. Then simulations were conducted for 2014-2017 for all sites. Empirical ANPP data were available from 2014-2017 for all sites, and BNPP was available for CPER, HPG, HAR, and KNZ for 2014-2017. BNPP was available at SBL and SBK from 2015-2017. To assess model performance, we calculated various validation metrics, including R2, RMSE, and the correlation coefficient.

Generally, cross-site averages of model output and observations were tightly correlated, but within-site model output was
865 less correlated to interannual empirical observations (Table 1). However, it is important to note the variation associated with empirical measurements and that most model simulations fell within one standard error of empirical observations (error bars in Fig. D2 and D3). A notable exception to this occurred in 2014 at CPER and HPG sites, where BNPP was observed as much greater than model simulations. We are unsure what drove the high BNPP at these sites in 2014 since environmental conditions were within normal ranges (Fig. D1). It could be that other unmeasured variables (e.g., belowground animal
870 activity, small mammal activity) were responsible for this high growth belowground.

Table D1. Model output for comparisons between empirical and simulated data.

Site	Productivity type	R2	RMSE	Correlation coefficient
means	anpp	0.988738	17.96882	0.994353
means	bnpp	0.93693	23.4836	0.967952

46

sbl	anpp	0.431519	9.568253	-0.6569
sbl	bnpp	0.009114	18.25828	-0.09547
sbk	anpp	0.667188	10.51358	0.816816
sbk	bnpp	0.059729	13.3254	-0.2444
cper	anpp	0.087017	33.30121	0.294986
cper	bnpp	0.181185	98.48398	0.425659
hpg	anpp	0.018955	35.10083	-0.13768
hpg	bnpp	0.022188	131.1703	0.148957
har	anpp	0.526963	28.82132	0.725922
har	bnpp	0.330895	34.27893	0.575235
knz	anpp	0.004173	162.8426	-0.0646
knz	bnpp	0.637154	36.67331	-0.79822

anpp=aboveground net primary productivity,
bnpp=belowground net primary productivity, sbl=Sevilleta
National Wildlife Refuge blue grama grassland;
sbk=Sevilleta National Wildlife Refuge black grama
grassland; cper=Central Plains Experimental Range;
hpg=High Plains Grasslands Research Station; har=Hays
Agricultural Research Center; knz=Konza Prairie Biological
Station
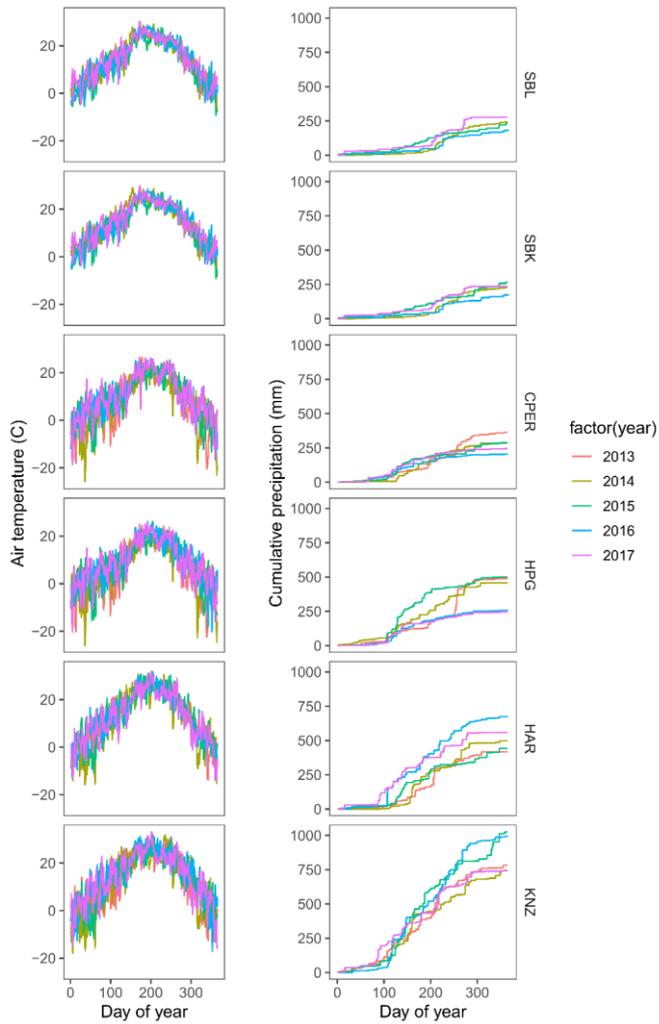
Figure D1. Cumulative hourly precipitation and hourly air temperature throughout each year simulated within each site.
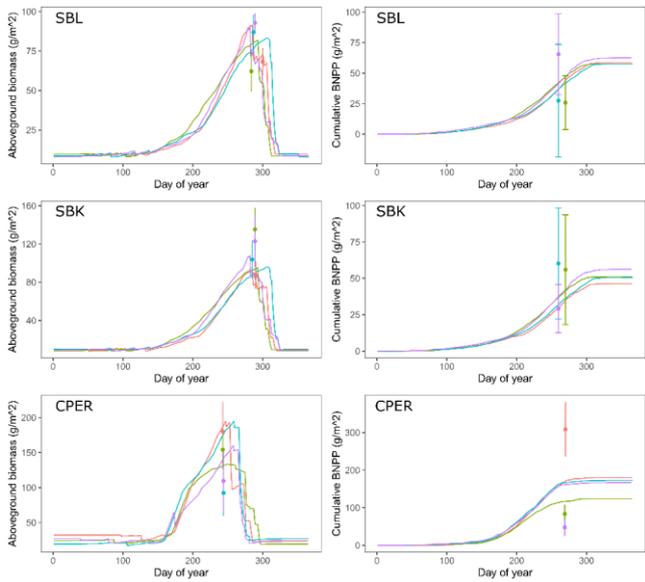
Figure D2. Within year patterns of simulated aboveground biomass and BNPP for SBL, SBK, and CPER, compared with empirical observations. Bars represent one standard deviation from the mean of the 10 replicate measurements. Years are represented as colors using the scale from Fig. 1.

880

885

890
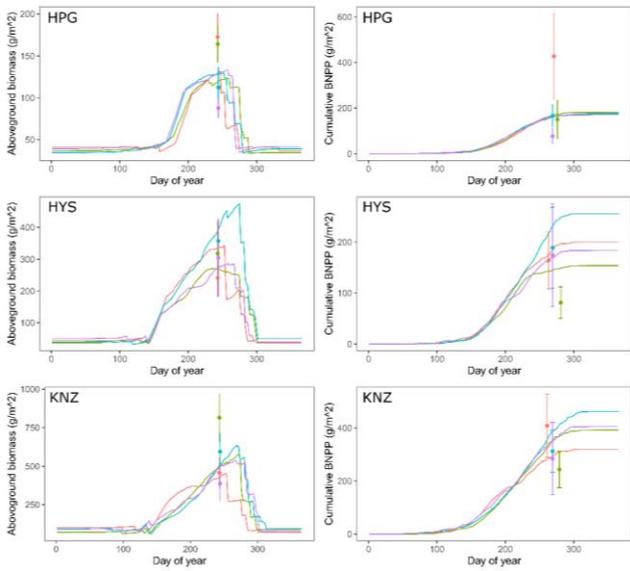
Figure D3. Within year patterns of simulated aboveground biomass and BNPP for HPG, HYS, and KNZ, compared with empirical observations. Bars represent one standard deviation from the mean of the 10 replicate measurements. Years are represented as colors using the scale from Fig. 1.

895

900

Appendix E. Land use history of study sites

Here, we outline the recent land use history starting with the establishment of the current associations responsible for managing these areas.

SBL, SBK: The Sevilleta National Wildlife Refuge in central New Mexico, USA, was established in 1973. Prior to that time the land was lightly to moderately grazed by domestic herbivores (mostly cattle along with some horses and sheep) for about three centuries as part of a collective land grant to settlers from the King of Spain. All domestic herbivores were removed from the site when the refuge was established, and the vegetation has recovered from grazing (Gosz and Gosz 1996, Collins and Xia 2015). The refuge sits at the intersection of several biomes (Gosz and Gosz 1996) including Great Plains grassland dominated by blue grama (Bouteloua gracilis)(SBL site in this study) and Chihuahuan Desert grassland dominated by black grama (B. eriopoda)(SBK site in this study). Chihuahuan Desert grassland is advancing northward into Great Plains grassland (Collins et al. 2020) in response to increasing aridity throughout the southwestern US (Rudgers et al. 2018, Maurer et al. 2020).

CPER: The Central Plains Experimental Range is a shortgrass prairie dominated by B. gracilis (Hazlett 1998). The experimental station was established in the 1930s to better understand how to manage lands to avoid catastrophic occurrences such as the Dust Bowl. A number of climatic and management effects occurred at CPER, including a severe blizzard in 1949, an extreme flood in 1965, and sever droughts in 1939, 1954, 1964 (Shoop et al. 1989), and 2012 (Knapp et al. 2015). The specific area where our plots were located have been ungrazed for 14 years prior to the start of measurements. Before then, grazing occurred in the area but fire was largely absent at the site.

HPG: The High Plains Grassland Research Station was authorized by congress in 1928 to experiment with various horticultural crops in arid lands, which was begun in 1930. In 1974, the station shifted focus to rangeland management, water conservation, and land reclamation. The area where the plots were located was ungrazed since 2004 (Dijkstra et al. 2010) and has little to no history of fire.

HAR: Kansas State University began management of The Agricultural Research Center-Hays in 1994 and was managed for cattle grazing. The plots where our plots were located were ungrazed and unburned since 2005 (Heisler-White et al. 2009).

KNZ: The land where Konza Prairie Biological Station resides was purchased by the Nature Conservancy in 1971 and deeded to Kansas State University to establish a watershed-scale experiment to assess the impacts of fire and grazing on tallgrass ecological processes (Knapp et al. 1998). The watershed where our measurements took place has been burned annually in the spring since 1988 and was ungrazed by large ungulates since the early 1980s.

Code availability

R scripts to conduct data assimilation, calculate all metrics presented in the paper and statistical analyses publically available at https://github.com/wilcoxkr/AssessingCarbonCapacity. TECO model code is available on the ECOLAB website here: https://www2.nau.edu/luo-lab/?downloads.

Data availability

MCMC chains and raw empirical data is available upon request to the corresponding author.

Author contributions

KRW, YL, MDS, SC, WP, and AKK designed the research project and participated in idea generation; KRW and ZS conducted analyses and model simulations; KRW led the writing process; all authors contributed to writing and editing process.

Competing interests

The authors declare that they have no conflict of interest

Acknowledgements

References

Adair, E.C., Parton, W.J., Del Grosso, S.J., Silver, W.L., Harmon, M.E., Hall, S.A., Burke, I.C. and Hart, S.C., 2008. Simple three‐pool model accurately describes patterns of long‐term litter decomposition in diverse climates. Global Change Biology, 14(11), pp.2636-2660.

Austin, A. T. and Vivanco, L.: Plant litter decomposition in a semi-arid ecosystem controlled by photodegradation, Nature, 442, 555–558, https://doi.org/10.1038/nature05038, 2006.

Baisden, W. T., Parfitt, R. L., Ross, C., Schipper, L. A., and Canessa, S.: Evaluating 50 years of time-series soil radiocarbon data: towards routine calculation of robust C residence times, Biogeochemistry, 112, 129–137, https://doi.org/10.1007/s10533-011-9675-y, 2013.

Balesdent, J., Wagner, G. H., and Mariotti, A.: Soil organic matter turnover in long-term field experiments as revealed by carbon-13 natural abundance, Soil Science Society of America Journal, 52, 118–124, 1988.

Bell, C., McIntyre, N., Cox, S., Tissue, D., and Zak, J.: Soil Microbial Responses to Temporal Variations of Moisture and Temperature in a Chihuahuan Desert Grassland, Microb Ecol, 56, 153–167, https://doi.org/10.1007/s00248-007-9333-z, 2008.

Bhattacharyya, S. S., Ros, G. H., Furtak, K., Iqbal, H. M. N., and Parra-Saldívar, R.: Soil carbon sequestration – An interplay between soil microbial community and soil organic matter dynamics, Science of The Total Environment, 815, 152928, https://doi.org/10.1016/j.scitotenv.2022.152928, 2022.

Bird, M. I., Chivas, A. R., and Head, J.: A latitudinal gradient in carbon turnover times in forest soils, Nature, 381, 143–146, 1996.

Blume, E., Bischoff, M., Reichert, J. M., Moorman, T., Konopka, A., and Turco, R. F.: Surface and subsurface microbial biomass, community structure and metabolic activity as a function of soil depth and season, Applied Soil Ecology, 20, 171–181, https://doi.org/10.1016/S0929-1393(02)00025-2, 2002.

Blumenthal, Dana; Kray, Julie; Mueller, Kevin; Ocheltree, Troy (2020), Shortgrass steppe and northern mixedgrass prairie plant species traits, Dryad, Dataset, https://doi.org/10.5061/dryad.8sf7m0cjr

Bonan, G.B., Hartman, M.D., Parton, W.J. and Wieder, W.R., 2013. Evaluating litter decomposition in earth system models with long‐term litterbag experiments: an example using the Community Land Model version 4 (CLM 4). Global change biology, 19(3), pp.957-974.

Bontti, E.E., Decant, J.P., Munson, S.M., Gathany, M.A., Przeszlowska, A., Haddix, M.L., Owens, S., Burke, I.C., Parton, W.J. and Harmon, M.E., 2009. Litter decomposition in grasslands of central North America (US Great Plains). Global Change Biology, 15(5), pp.1356-1363.

Brandt, L. A., King, J. Y., Hobbie, S. E., Milchunas, D. G., and Sinsabaugh, R. L.: The Role of Photodegradation in Surface Litter Decomposition Across a Grassland Ecosystem Precipitation Gradient, Ecosystems, 13, 765–781, https://doi.org/10.1007/s10021-010-9353-2, 2010.

Burke, I.C., Lauenroth, W.K. and Parton, W.J., 1997. Regional and temporal variation in net primary production and nitrogen mineralization in grasslands. Ecology, 78(5), pp.1330-1340.

Carvalhais, N., Forkel, M., Khomik, M., Bellarby, J., Jung, M., Migliavacca, M., Mu, M., Saatchi, S., Santoro, M., Thurner, M., Weber, U., Ahrens, B., Beer, C., Cescatti, A., Randerson, J. T., and Reichstein, M.: Global covariation of carbon turnover times with climate in terrestrial ecosystems, Nature, 514, 213–217, https://doi.org/10.1038/nature13731, 2014.

Chambers, A., Lal, R. and Paustian, K., 2016. Soil carbon sequestration potential of US croplands and grasslands: Implementing the 4 per Thousand Initiative. Journal of Soil and Water Conservation, 71(3), pp.68A-74A.

Chapin III, F. S., Matson, P. A., and Mooney, H. A.: Principles of Terrestrial Ecosystem Ecology, Springer-Verlag New York, Inc, New York, NY, 2011.

Chen, S., Huang, Y., Zou, J., and Shi, Y.: Mean residence time of global topsoil organic carbon depends on temperature, precipitation and soil nitrogen, Global and Planetary Change, 100, 99–108, https://doi.org/10.1016/j.gloplacha.2012.10.006, 2013.

Collins, S. L., Sinsabaugh, R. L., Crenshaw, C., Green, L., Porras-Alfaro, A., Stursova, M., and Zeglin, L. H.: Pulse dynamics and microbial processes in aridland ecosystems: Pulse dynamics in aridland soils, Journal of Ecology, 96, 413–420, https://doi.org/10.1111/j.1365-2745.2008.01362.x, 2008.

Conant RT, Cerri CE, Osborne BB, Paustian K. Grassland management impacts on soil carbon stocks: a new synthesis. Ecological Applications. 2017 Mar;27(2):662-8.

Conant, R.T., Ryan, M.G., Ågren, G.I., Birge, H.E., Davidson, E.A., Eliasson, P.E., Evans, S.E., Frey, S.D., Giardina, C.P., Hopkins, F.M. and Hyvönen, R., 2011. Temperature and soil organic matter decomposition rates–synthesis of current knowledge and a way forward. Global change biology, 17(11), pp.3392-3404.

Daily, G. C., Polasky, S., Goldstein, J., Kareiva, P. M., Mooney, H. A., Pejchar, L., Ricketts, T. H., Salzman, J., and Shallenberger, R.: Ecosystem services in decision making: time to deliver, Frontiers in Ecology and the Environment, 7, 21–28, https://doi.org/10.1890/080025, 2009.

De Kauwe, M. G., Medlyn, B. E., Zaehle, S., Walker, A. P., Dietze, M. C., Wang, Y., Luo, Y., Jain, A. K., El-Masri, B., Hickler, T., Wårlind, D., Weng, E., Parton, W. J., Thornton, P. E., Wang, S., Prentice, I. C., Asao, S., Smith, B., McCarthy, H. R., Iversen, C. M., Hanson, P. J., Warren, J. M., Oren, R., and Norby, R. J.: Where does the carbon go? A model–data intercomparison of vegetation carbon allocation and turnover processes at two temperate forest free-air CO_2 enrichment sites, New Phytol, 203, 883–899, https://doi.org/10.1111/nph.12847, 2014.

Doetterl, S., Stevens, A., Six, J., Merckx, R., Van Oost, K., Casanova Pinto, M., Casanova-Katny, A., Muñoz, C., Boudin, M., Zagal Venegas, E., and Boeckx, P.: Soil carbon storage controlled by interactions between geochemistry and climate, Nature Geosci, 8, 780–783, https://doi.org/10.1038/ngeo2516, 2015.

Feng, J., Wang, J., Song, Y., and Zhu, B.: Patterns of soil respiration and its temperature sensitivity in grassland ecosystems across China, Biogeosciences, 15, 5329–5341, https://doi.org/10.5194/bg-15-5329-2018, 2018.

Fierer, N. and Schimel, J. P.: Effects of drying–rewetting frequency on soil carbon and nitrogen transformations, Soil Biology and Biochemistry, 34, 777–787, https://doi.org/10.1016/S0038-0717(02)00007-X, 2002.

Fierer, N., Schimel, J. P., and Holden, P. A.: Variations in microbial community composition through two soil depth profiles, Soil Biology and Biochemistry, 35, 167–176, https://doi.org/10.1016/S0038-0717(02)00251-1, 2003.

Freckleton, R. P.: The problems of prediction and scale in applied ecology: the example of fire as a management tool: Editorial, Journal of Applied Ecology, 41, 599–603, https://doi.org/10.1111/j.0021-8901.2004.00941.x, 2004.

Friend, A. D., Lucht, W., Rademacher, T. T., Keribin, R., Betts, R., Cadule, P., Ciais, P., Clark, D. B., Dankers, R., Falloon, P. D., Ito, A., Kahana, R., Kleidon, A., Lomas, M. R., Nishina, K., Ostberg, S., Pavlick, R., Peylin, P., Schaphoff, S., Vuichard, N., Warszawski, L., Wiltshire, A., and Woodward, F. I.: Carbon residence time dominates uncertainty in terrestrial vegetation responses to future climate and atmospheric CO_2, Proc. Natl. Acad. Sci. U.S.A., 111, 3280–3285, https://doi.org/10.1073/pnas.1222477110, 2014.

García-Palacios, P., Shaw, E. A., Wall, D. H., and Hättenschwiler, S.: Temporal dynamics of biotic and abiotic drivers of litter decomposition, Ecol Lett, 19, 554–563, https://doi.org/10.1111/ele.12590, 2016.

Guzman, J. G. and Al-Kaisi, M. M.: Soil Carbon Dynamics and Carbon Budget of Newly Reconstructed Tall-grass Prairies in South Central Iowa, J. Environ. Qual., 39, 136–146, https://doi.org/10.2134/jeq2009.0063, 2010.

Harmon, M.E., Silver, W.L., Fasth, B., Chen, H.U.A., Burke, I.C., Parton, W.J., Hart, S.C., Currie, W.S. and Lidet, 2009. Long‐term patterns of mass loss during the decomposition of leaf and fine root litter: an intersite comparison. Global Change Biology, 15(5), pp.1320-1338.

Holguin, J., Collins, S.L. and McLaren, J.R., 2022. Belowground responses to altered precipitation regimes in two semi-arid grasslands. Soil Biology and Biochemistry, 171, p.108725.

Hou, E., Rudgers, J.A., Collins, S.L., Litvak, M.E., White, C.S., Moore, D.I. and Luo, Y., 2021. Sensitivity of soil organic matter to climate and fire in a desert grassland. Biogeochemistry, 156, pp.59-74.

Hu, Z., Song, X., Wang, M., Ma, J., Zhang, Y., Xu, H.-J., Hu, Z., Zhu, X., Liu, H., Ma, J., Yu, Q., Ostle, N. J., Li, Y., and Yue, C.: Aridity influences root versus shoot contributions to steppe grassland soil carbon stock and its stability, Geoderma, 413, 115744, https://doi.org/10.1016/j.geoderma.2022.115744, 2022.

54

Hungate, B. A., Holland, E. A., Jackson, R. B., Chapin, F. S., Mooney, H. A., and Field, C. B.: The fate of carbon in grasslands under carbon dioxide enrichment, Nature, 388, 576–579, https://doi.org/10.1038/41550, 1997.

Huxman, T. E., Smith, M. D., Fay, P. A., Knapp, A. K., Shaw, M. R., Loik, M. E., Smith, S. D., Tissue, D. T., Zak, J. C., Weltzin, J. F., Pockman, W. T., Sala, O. E., Haddad, B. M., Harte, J., Koch, G. W., Schwinning, S., Small, E. E., and Williams, D. G.: Convergence across biomes to a common rain-use efficiency, Nature, 429, 651–654, https://doi.org/10.1038/nature02561, 2004.

IPCC, 2022: Summary for Policymakers [H.-O. Pörtner, D.C. Roberts, E.S. Poloczanska, K. Mintenbeck, M. Tignor, A. Alegría, M. Craig, S. Langsdorf, S. Löschke, V. Möller, A. Okem (eds.)]. In: Climate Change 2022: Impacts, Adaptation and Vulnerability. Contribution of Working Group II to the Sixth Assessment Report of the Intergovernmental Panel on Climate Change [H.-O. Pörtner, D.C. Roberts, M. Tignor, E.S. Poloczanska, K. Mintenbeck, A. Alegría, M. Craig, S. Langsdorf, S. Löschke, V. Möller, A. Okem, B. Rama (eds.)]. Cambridge University Press, Cambridge, UK and New York, NY, USA, pp. 3–33, doi:10.1017/9781009325844.001.

Jackson, R. B., Canadell, J., Ehleringer, J. R., Mooney, H. A., Sala, O. E., and Schulze, E. D.: A global analysis of root distributions for terrestrial biomes, Oecologia, 108, 389–411, https://doi.org/10.1007/BF00333714, 1996.

Jobbágy, E. G. and Jackson, R. B.: THE VERTICAL DISTRIBUTION OF SOIL ORGANIC CARBON AND ITS RELATION TO CLIMATE AND VEGETATION, Ecological Applications, 10, 14, 2000.

Johnson, L. C. and Matchett, J. R.: FIRE AND GRAZING REGULATE BELOWGROUND PROCESSES IN TALLGRASS PRAIRIE, Ecology, 82, 3377–3389, https://doi.org/10.1890/0012-9658(2001)082[3377:FAGRBP]2.0.CO;2, 2001.

Knapp, A. K., Briggs, J. M., Hartnett, D. C., and Collins, S. L.: Grassland dynamics: Long-term ecological research in tallgrass prairie, Oxford University Press, Inc., New York, NY, 1998.

Knapp, A. K., Carroll, C. J. W., Denton, E. M., La Pierre, K. J., Collins, S. L., and Smith, M. D.: Differential sensitivity to regional-scale drought in six central US grasslands, Oecologia, 177, 949–957, https://doi.org/10.1007/s00442-015-3233-6, 2015.

Lal, R.: Soil Carbon Sequestration Impacts on Global Climate Change and Food Security, Science, 304, 1623–1627, https://doi.org/10.1126/science.1097396, 2004.

Leppälammi-Kujansuu, J., Aro, L., Salemaa, M., Hansson, K., Kleja, D. B., and Helmisaari, H.-S.: Fine root longevity and carbon input into soil from below- and aboveground litter in climatically contrasting forests, Forest Ecology and Management, 326, 79–90, https://doi.org/10.1016/j.foreco.2014.03.039, 2014.

Liski, J., Ilvesniemi, H., Mäkelä, A. and Westman, C.J., 1999. CO_2 emissions from soil in response to climatic warming are overestimated: the decomposition of old soil organic matter is tolerant of temperature. Ambio, pp.171-174.

Lorenz, K., Lal, R., Lorenz, K. and Lal, R., 2018. Carbon sequestration in grassland soils. Carbon sequestration in agricultural ecosystems, pp.175-209.

Luo, Y., Keenan, T. F., and Smith, M.: Predictability of the terrestrial carbon cycle, Glob Change Biol, 21, 1737–1751, https://doi.org/10.1111/gcb.12766, 2015.

Luo, Y., Shi, Z., Lu, X., Xia, J., Liang, J., Jiang, J., Wang, Y., Smith, M. J., Jiang, L., Ahlström, A., Chen, B., Hararuk, O., Hastings, A., Hoffman, F., Medlyn, B., Niu, S., Rasmussen, M., Todd-Brown, K., and Wang, Y.-P.: Transient dynamics of terrestrial carbon storage: mathematical foundation and its applications, Biogeosciences, 14, 145–161, https://doi.org/10.5194/bg-14-145-2017, 2017.

Mathieu, J. A., Hatté, C., Balesdent, J., and Parent, É.: Deep soil carbon dynamics are driven more by soil type than by climate: a worldwide meta-analysis of radiocarbon profiles, Glob Change Biol, 21, 4278–4292, https://doi.org/10.1111/gcb.13012, 2015.

Maurer, G. E., Hallmark, A. J., Brown, R. F., Sala, O. E., and Collins, S. L.: Sensitivity of primary production to precipitation across the United States, Ecol Lett, 23, 527–536, https://doi.org/10.1111/ele.13455, 2020.

Mokany, K., Raison, R. J., and Prokushkin, A. S.: Critical analysis of root : shoot ratios in terrestrial biomes: ROOT : SHOOT RATIOS IN TERRESTRIAL BIOMES, Global Change Biology, 12, 84–96, https://doi.org/10.1111/j.1365-2486.2005.001043.x, 2006.

Moore, S., Adu-Bredu, S., Duah-Gyamfi, A., Addo-Danso, S. D., Ibrahim, F., Mbou, A. T., Grandcourt, A., Valentini, R., Nicolini, G., Djagbletey, G., Owusu-Afriyie, K., Gvozdevaite, A., Oliveras, I., Ruiz-Jaen, M. C., and Malhi, Y.: Forest biomass, productivity and carbon cycling along a rainfall gradient in West Africa, Glob Change Biol, 24, e496–e510, https://doi.org/10.1111/gcb.13907, 2018.

Luke Nave, Kris Johnson, Catharine van Ingen, Deborah Agarwal, Marty Humphrey, and Norm Beekwilder, International Soil Carbon Network (ISCN) Database V3-1, 10.17040/ISCN/1305039. Accessed July 2017.

Naylor, D., Sadler, N., Bhattacharjee, A., Graham, E. B., Anderton, C. R., McClure, R., Lipton, M., Hofmockel, K. S., and Jansson, J. K.: Soil Microbiomes Under Climate Change and Implications for Carbon Cycling, Annu. Rev. Environ. Resour., 45, 29–59, https://doi.org/10.1146/annurev-environ-012320-082720, 2020.

Ojima, D.S., Schimel, D.S., Parton, W.J. and Owensby, C.E., 1994. Long-and short-term effects of fire on nitrogen cycling in tallgrass prairie. Biogeochemistry, 24, pp.67-84.

Jari Oksanen, Gavin L. Simpson, F. Guillaume Blanchet, Roeland Kindt, Pierre Legendre, Peter R. Minchin, R.B. O'Hara, Peter Solymos, M. Henry H. Stevens, Eduard Szoecs, Helene Wagner, Matt Barbour, Michael Bedward, Ben Bolker, Daniel Borcard, Gustavo Carvalho, Michael Chirico, Miquel De Caceres, Sebastien Durand, Heloisa Beatriz Antoniazi Evangelista, Rich FitzJohn, Michael Friendly, Brendan Furneaux, Geoffrey Hannigan, Mark O. Hill, Leo Lahti, Dan McGlinn, Marie-Helene Ouellette, Eduardo Ribeiro Cunha, Tyler Smith, Adrian Stier, Cajo J.F. Ter Braak and James Weedon (2022). vegan: Community Ecology Package. R package version 2.6-2. https://CRAN.R-project.org/package=vegan

Pan, Y., Birdsey, R. A., Fang, J., Houghton, R., Kauppi, P. E., Kurz, W. A., Phillips, O. L., Shvidenko, A., Lewis, S. L., Canadell, J. G., Ciais, P., Jackson, R. B., Pacala, S. W., McGuire, A. D., Piao, S., Rautiainen, A., Sitch, S., and Hayes, D.: A Large and Persistent Carbon Sink in the World's Forests, Science, 333, 988–993, https://doi.org/10.1126/science.1201609, 2011.

Parton, W.J., Scurlock, J.M.O., Ojima, D.S., Gilmanov, T.G., Scholes, R.J., Schimel, D.S., Kirchner, T., Menaut, J.C., Seastedt, T., Garcia Moya, E. and Kamnalrut, A., 1993. Observations and modeling of biomass and soil organic matter dynamics for the grassland biome worldwide. Global biogeochemical cycles, 7(4), pp.785-809.

Parton, W., Silver, W. L., Burke, I. C., Grassens, L., Harmon, M. E., Currie, W. S., King, J. Y., Adair, E. C., Brandt, L. A., Hart, S. C., and Fasth, B.: Global-Scale Similarities in Nitrogen Release Patterns During Long-Term Decomposition, Science, 315, 361–364, https://doi.org/10.1126/science.1134853, 2007.

Petrie, M. D., Collins, S. L., Swann, A. M., Ford, P. L., and Litvak, M. E.: Grassland to shrubland state transitions enhance carbon sequestration in the northern Chihuahuan Desert, Global Change Biology, 21, 1226–1235, https://doi.org/10.1111/gcb.12743, 2015.

Poulter, B., Frank, D., Ciais, P., Myneni, R. B., Andela, N., Bi, J., Broquet, G., Canadell, J. G., Chevallier, F., Liu, Y. Y., Running, S. W., Sitch, S., and van der Werf, G. R.: Contribution of semi-arid ecosystems to interannual variability of the global carbon cycle, Nature, 509, 600–603, https://doi.org/10.1038/nature13376, 2014.

1125 R Core Team (2022). R: A language and environment for statistical computing. R Foundation for Statistical Computing, Vienna, Austria. https://www.R-project.org/

Rees, R. M., Bingham, I. J., Baddeley, J. A., and Watson, C. A.: The role of plants and land management in sequestering soil carbon in temperate arable and grassland ecosystems, Geoderma, 128, 130–154, https://doi.org/10.1016/j.geoderma.2004.12.020, 2005.

1130 Rudgers, J.A., Hallmark, A., Baker, S.R., Baur, L., Hall, K.M., Litvak, M.E., Muldavin, E.H., Pockman, W.T. and Whitney, K.D., 2019. Sensitivity of dryland plant allometry to climate. Functional Ecology, 33(12), pp.2290-2303.

Saiz, G., Bird, M. I., Domingues, T., Schrodt, F., Schwarz, M., Feldpausch, T. R., Veenendaal, E., Djagbletey, G., Hien, F., Compaore, H., Diallo, A., and Lloyd, J.: Variation in soil carbon stocks and their determinants across a precipitation gradient in West Africa, Glob Change Biol, 18, 1670–1683, https://doi.org/10.1111/j.1365-2486.2012.02657.x, 2012.

1135 Sala, O. E., Parton, W. J., Joyce, L. A., and Lauenroth, W. K.: Primary Production of the Central Grassland Region of the United States, Ecology, 69, 40–45, https://doi.org/10.2307/1943158, 1988.

Sala, O. E., Gherardi, L. A., Reichmann, L., Jobbágy, E., and Peters, D.: Legacies of precipitation fluctuations on primary production: theory and data synthesis, Phil. Trans. R. Soc. B, 367, 3135–3144, https://doi.org/10.1098/rstb.2011.0347, 2012.

Schenk, H. J. and Jackson, R. B.: THE GLOBAL BIOGEOGRAPHY OF ROOTS, Ecological Monographs, 72, 311–328,
1140 https://doi.org/10.1890/0012-9615(2002)072[0311:TGBOR]2.0.CO;2, 2002.

Seastedt, T. R.: Mass, Nitrogen, and Phosphorus Dynamics in Foliage and Root Detritus of Tallgrass Prairie, Ecology, 69, 59–65, https://doi.org/10.2307/1943160, 1988.

Shi, Z., Thomey, M. L., Mowll, W., Litvak, M., Brunsell, N. A., Collins, S. L., Pockman, W. T., Smith, M. D., Knapp, A. K., and Luo, Y.: Differential effects of extreme drought on production and respiration: synthesis and modeling analysis,
1145 Biogeosciences, 11, 621–633, https://doi.org/10.5194/bg-11-621-2014, 2014.

Shi, Z., Xu, X., Hararuk, O., Jiang, L., Xia, J., Liang, J., Li, D., and Luo, Y.: Experimental warming altered rates of carbon processes, allocation, and carbon storage in a tallgrass prairie, Ecosphere, 6, art210, https://doi.org/10.1890/ES14-00335.1, 2015.

Sinsabaugh, R. L., Lauber, C. L., Weintraub, M. N., Ahmed, B., Allison, S. D., Crenshaw, C., Contosta, A. R., Cusack, D.,
1150 Frey, S., Gallo, M. E., Gartner, T. B., Hobbie, S. E., Holland, K., Keeler, B. L., Powers, J. S., Stursova, M., Takacs-Vesbach, C., Waldrop, M. P., Wallenstein, M. D., Zak, D. R., and Zeglin, L. H.: Stoichiometry of soil enzyme activity at global scale: Stoichiometry of soil enzyme activity, Ecology Letters, 11, 1252–1264, https://doi.org/10.1111/j.1461-0248.2008.01245.x, 2008.

Smith, P., 2004. Carbon sequestration in croplands: the potential in Europe and the global context. European journal of
1155 agronomy, 20(3), pp.229-236.

Smith, P., Andrén, O., Karlsson, T., Perälä, P., Regina, K., Rounsevell, M. and Van Wesemael, B., 2005. Carbon sequestration potential in European croplands has been overestimated. Global Change Biology, 11(12), pp.2153-2163.

Smith, P.: Do grasslands act as a perpetual sink for carbon?, Glob Change Biol, 20, 2708–2711, https://doi.org/10.1111/gcb.12561, 2014.

57

1160 Soong, J. L. and Cotrufo, M. F.: Annual burning of a tallgrass prairie inhibits C and N cycling in soil, increasing recalcitrant pyrogenic organic matter storage while reducing N availability, Glob Change Biol, 21, 2321–2333, https://doi.org/10.1111/gcb.12832, 2015.

Soussana, J. F., Allard, V., Pilegaard, K., Ambus, P., Amman, C., Campbell, C., Ceschia, E., Clifton-Brown, J., Czobel, S., Domingues, R., Flechard, C., Fuhrer, J., Hensen, A., Horvath, L., Jones, M., Kasper, G., Martin, C., Nagy, Z., Neftel, A., 1165 Raschi, A., Baronti, S., Rees, R. M., Skiba, U., Stefani, P., Manca, G., Sutton, M., Tuba, Z., and Valentini, R.: Full accounting of the greenhouse gas (CO2, N2O, CH4) budget of nine European grassland sites, Agriculture, Ecosystems & Environment, 121, 121–134, https://doi.org/10.1016/j.agee.2006.12.022, 2007.

Sperow, M., 2016. Estimating carbon sequestration potential on US agricultural topsoils. Soil and Tillage Research, 155, pp.390-400.

1170 Stielstra, C. M., Lohse, K. A., Chorover, J., McIntosh, J. C., Barron-Gafford, G. A., Perdrial, J. N., Litvak, M., Barnard, H. R., and Brooks, P. D.: Climatic and landscape influences on soil moisture are primary determinants of soil carbon fluxes in seasonally snow-covered forest ecosystems, Biogeochemistry, 123, 447–465, https://doi.org/10.1007/s10533-015-0078-3, 2015.

Sulman, B. N., Moore, J. A. M., Abramoff, R., Averill, C., Kivlin, S., Georgiou, K., Sridhar, B., Hartman, M. D., Wang, G., 1175 Wieder, W. R., Bradford, M. A., Luo, Y., Mayes, M. A., Morrison, E., Riley, W. J., Salazar, A., Schimel, J. P., Tang, J., and Classen, A. T.: Multiple models and experiments underscore large uncertainty in soil carbon dynamics, Biogeochemistry, 141, 109–123, https://doi.org/10.1007/s10533-018-0509-z, 2018.

Sulzman, E. W., Brant, J. B., Bowden, R. D., and Lajtha, K.: Contribution of aboveground litter, belowground litter, and rhizosphere respiration to total soil CO2 efflux in an old growth coniferous forest, Biogeochemistry, 73, 231–256, 1180 https://doi.org/10.1007/s10533-004-7314-6, 2005.

Taylor, J. P., Wilson, B., Mills, M. S., and Burns, R. G.: Comparison of microbial numbers and enzymatic activities in surface soils and subsoils using various techniques, Soil Biology and Biochemistry, 34, 387–401, https://doi.org/10.1016/S0038-0717(01)00199-7, 2002.

Telles, E. de C. C., de Camargo, P. B., Martinelli, L. A., Trumbore, S. E., da Costa, E. S., Santos, J., Higuchi, N., and 1185 Oliveira, R. C.: Influence of soil texture on carbon dynamics and storage potential in tropical forest soils of Amazonia: CARBON STORAGE POTENTIAL OF TROPICAL SOILS, Global Biogeochem. Cycles, 17, n/a-n/a, https://doi.org/10.1029/2002GB001953, 2003.

Thomey, M. L., Collins, S. L., Vargas, R., Johnson, J. E., Brown, R. F., Natvig, D. O., and Friggens, M. T.: Effect of precipitation variability on net primary production and soil respiration in a Chihuahuan Desert grassland: PRECIPITATION 1190 VARIABILITY IN DESERT GRASSLAND, Global Change Biology, 17, 1505–1515, https://doi.org/10.1111/j.1365-2486.2010.02363.x, 2011.

Todd-Brown, K. E. O., Randerson, J. T., Hopkins, F., Arora, V., Hajima, T., Jones, C., Shevliakova, E., Tjiputra, J., Volodin, E., Wu, T., Zhang, Q., and Allison, S. D.: Changes in soil organic carbon storage predicted by Earth system models during the 21st century, Biogeosciences, 11, 2341–2356, https://doi.org/10.5194/bg-11-2341-2014, 2014.

1195 Wang, Y., Xie, Z., and Jia, B.: Incorporation of a dynamic root distribution into CLM4.5: Evaluation of carbon and water fluxes over the Amazon, Adv. Atmos. Sci., 33, 1047–1060, https://doi.org/10.1007/s00376-016-5226-8, 2016.

Weng, E. and Luo, Y.: Soil hydrological properties regulate grassland ecosystem responses to multifactor global change: A modeling analysis, J. Geophys. Res., 113, G03003, https://doi.org/10.1029/2007JG000539, 2008.

Formatted: Superscript

Wiesmeier, M., Urbanski, L., Hobley, E., Lang, B., von Lützow, M., Marin-Spiotta, E., van Wesemael, B., Rabot, E., Ließ, M., Garcia-Franco, N., Wollschläger, U., Vogel, H.-J., and Kögel-Knabner, I.: Soil organic carbon storage as a key function of soils - A review of drivers and indicators at various scales, Geoderma, 333, 149–162, https://doi.org/10.1016/j.geoderma.2018.07.026, 2019.

Wilcox, K. R., Blair, J. M., and Knapp, A. K.: Stability of grassland soil C and N pools despite 25 years of an extreme climatic and disturbance regime: PRECIPITATION IMPACTS ON SOIL C AND N, J. Geophys. Res. Biogeosci., 121, 1934–1945, https://doi.org/10.1002/2016JG003370, 2016.

Williams, M. A. and Rice, C. W.: Seven years of enhanced water availability influences the physiological, structural, and functional attributes of a soil microbial community, Applied Soil Ecology, 35, 535–545, https://doi.org/10.1016/j.apsoil.2006.09.014, 2007.

Wu, D., Piao, S., Zhu, D., Wang, X., Ciais, P., Bastos, A., Xu, X., and Xu, W.: Accelerated terrestrial ecosystem carbon turnover and its drivers, Glob Change Biol, 26, 5052–5062, https://doi.org/10.1111/gcb.15224, 2020.

Wu, Z., Dijkstra, P., Koch, G. W., Peñuelas, J., and Hungate, B. A.: Responses of terrestrial ecosystems to temperature and precipitation change: a meta-analysis of experimental manipulation: META-ANALYSIS OF EXPERIMENTAL MANIPULATION, Global Change Biology, 17, 927–942, https://doi.org/10.1111/j.1365-2486.2010.02302.x, 2011.

Xu, T., White, L., Hui, D., and Luo, Y.: Probabilistic inversion of a terrestrial ecosystem model: Analysis of uncertainty in parameter estimation and model prediction: PROBABILISTIC INVERSION OF TERRESTRIAL ECOSYSTEM, Global Biogeochem. Cycles, 20, n/a-n/a, https://doi.org/10.1029/2005GB002468, 2006.

Yahdjian, L., Sala, O.E. and Austin, A.T., 2006. Differential controls of water input on litter decomposition and nitrogen dynamics in the Patagonian steppe. Ecosystems, 9, pp.128-141.

You, Y., Wang, J., Huang, X., Tang, Z., Liu, S., and Sun, O. J.: Relating microbial community structure to functioning in forest soil organic carbon transformation and turnover, Ecol Evol, 4, 633–647, https://doi.org/10.1002/ece3.969, 2014.

Zhao, Y. F., Wang, X., Jiang, S. L., Zhou, X. H., Liu, H. Y., Xiao, J. J., Hao, Z. G., and Wang, K. C.: Climate and geochemistry interactions at different altitudes influence soil organic carbon turnover times in alpine grasslands, Agriculture, Ecosystems & Environment, 320, 107591, https://doi.org/10.1016/j.agee.2021.107591, 2021.

Zhou, T. and Luo, Y.: Spatial patterns of ecosystem carbon residence time and NPP-driven carbon uptake in the conterminous United States: CARBON RESIDENCE TIME AND CARBON UPTAKE, Global Biogeochem. Cycles, 22, n/a-n/a, https://doi.org/10.1029/2007GB002939, 2008.

Zhou, X., Talley, M. and Luo, Y., 2009. Biomass, litter, and soil respiration along a precipitation gradient in southern Great Plains, USA. Ecosystems, 12, pp.1369-1380.

Zhou, X., Zhou, T., and Luo, Y.: Uncertainties in carbon residence time and NPP-driven carbon uptake in terrestrial ecosystems of the conterminous USA: a Bayesian approach, Tellus B: Chemical and Physical Meteorology, 64, 17223, https://doi.org/10.3402/tellusb.v64i0.17223, 2012.